KAPL-4756
UC-901, Chemistry

Magnetite Solubility and Phase Stability in Alkaline Media at Elevated Temperatures

S. E. Ziemniak

M. E. Jones

K. E. S. Combs

Prepared for
The United States Department of Energy

Prepared by
KNOLLS ATOMIC POWER LABORATORY
Schenectady, New York
Contract DE-AC12-76-SN00052

DISCLAIMER

ABSTRACT

A platinum-lined, flowing autoclave facility was used to investigate the solubility behavior of magnetite (Fe_3O_4) in alkaline sodium phosphate and ammonium hydroxide solutions between 21 and 288°C. Measured iron solubilities were interpreted via a Fe(II)/Fe(III) ion hydroxo-, phosphato-, and ammino-complexing model and thermodynamic functions for these equilibria were obtained from a least-squares analysis of the data. A total of 14 iron ion species were fitted. Complexing equilibria are reported for 8 new species: $Fe(OH)(NH_3)^+$, $Fe(OH)(HPO_4)^-$, $Fe(OH)_2(HPO_4)^{2-}$, $Fe(OH)_2(PO_4)^{3-}$, $Fe(OH)_3(HPO_4)^{2-}$, $Fe(OH)_4(HPO_4)^{3-}$, $Fe(OH)_2(H_2PO_4)^-$, and $Fe(OH)_3(H_2PO_4)^-$. $Fe(OH)_n(HPO_4)^{n-}$ complexes were stabilized at low temperatures, while $Fe(OH)_m(HPO_4)^{1-m}$ complexes were stabilized at elevated temperatures. Magnetite solubilities were controlled by a surface layer of hydrous Fe(II) oxide at temperatures below 83°C for a dissolved hydrogen concentration of 234 μmol/kg. The level of dissolved hydrogen was shown to affect the $Fe(OH)_2/Fe_3O_4$ transformation temperature as well as the Fe(II)/Fe(III) redox equilibria.

KEY WORDS: Magnetite; iron oxide; aqueous solutions; ferrous ion hydrolysis; ferric ion hydrolysis; phosphatocomplexing; equilibrium constant; thermodynamics; pressurized water; hydrothermal solutions; corrosion.

ACKNOWLEDGEMENT

We are indebted to the following individuals who provided magnetite characterization analyses: G. M. Neugebauer - scanning electron microscopy; P. C. Sander - X-ray diffraction; T. A. DeVito - Mössbauer spectroscopy; and J. Chera (GE Corporate Research and Development Center) - X-ray photoelectron spectroscopy. H. J. Schermerhorn prepared the magnetite particles used in this study.

CONTENTS

ILLUSTRATIONS

TABLES

MAGNETITE SOLUBILITY AND PHASE STABILITY IN ALKALINE SODIUM PHOSPHATE SOLUTIONS AT ELEVATED TEMPERATURES

INTRODUCTION

Magnetite, Fe_3O_4, is the dominant oxide constituent of the indigenous corrosion layers that form on iron base alloys in high purity, high temperature water. The apparent simultaneous stability of two distinct oxidation states of iron in this metal oxide is responsible for its unique solubility behavior. As first demonstrated by Sweeton and Baes[1], a reductive dissolution is observed in acidic and mildly alkaline solutions:

$$\tfrac{1}{3} Fe_3O_4(s) + (2-n)H^+ + \tfrac{1}{3} H_2(g) \rightleftharpoons Fe(OH)_n^{2-n} + (\frac{4}{3} - n) H_2O \qquad (1)$$

where $0 \leq n \leq 3$. In solutions of higher alkalinity, Tremaine and LeBlanc[2] concluded that an oxidative dissolution occurs:

$$\tfrac{1}{3} Fe_3O_4(s) + (3-m)H^+ \rightleftharpoons Fe(OH)_m^{3-m} + \frac{1}{6} H_2(g) + (\frac{4}{3} - m)H_2O \qquad (2)$$

where $m \geq 3$. Therefore, in certain ranges of alkalinity where an overlap occurs ($n = 2, 3$ and $m = 3, 4$), dissolved hydrogen (or oxygen) levels play a significant role in determining the controlling soluble species. For example, iron solubilities will <u>increase</u> in proportion to $\{P(H_2)\}^{1/3}$ when Fe(II) species dominate, whereas they will <u>decrease</u> in proportion to $\{P(H_2)\}^{-1/6}$ when Fe(III) species dominate.

The above behavior is possible because hydrolysis is a metal ion stabilizing process, and the Fe(III) state hydrolyzes more readily than the Fe(II) state. Thus, a point is reached

in weakly alkaline pH solutions where stability of the $Fe(OH)_3(aq)$ hydroxocomplex approaches that of the $Fe(OH)_2(aq)$ hydroxocomplex. By means of magnetite solubility studies conducted in sodium hydroxide with varying levels of dissolved hydrogen, Tremaine and LeBlanc[2] quantified the redox equilibrium:

$$Fe(OH)_2(aq) + H_2O \rightleftharpoons Fe(OH)_3(aq) + \tfrac{1}{2}H_2(g) \qquad (3)$$

as $\Delta G(T)$, J/mol = 28623 - 35.73T. The temperature sensitivity of this equilibrium, together with decreases in hydrogen partial pressure at elevated temperatures, allows the $Fe(OH)_3(aq)/Fe(OH)_2(aq)$ concentration ratio to approach 3/7 at 300°C in solutions saturated with one atmosphere of hydrogen gas at room temperature, i.e., 779 μmol H_2/kg. Likewise, in solutions of higher alkalinity, the same level of dissolved hydrogen leads to $Fe(OH)_4^-/Fe(OH)_3^-$ concentration ratios greater than unity at temperatures above 166°C.

The present work was undertaken to extend the experimental and theoretical bases for estimating solubilities of an iron corrosion product ($Fe_3O_4/Fe(OH)_2$) over a broader temperature range and in the presence of complexing, pH-controlling reagents. Our results indicate that a surface layer of ferrous hydroxide controls magnetite solubility behavior at low temperatures in much the same manner as a surface layer of nickel(II) hydroxide was previously reported to control the low temperature solubility behavior of NiO[3]. The importance of Fe(III) ion complexes implies not only that most previously-derived thermodynamic properties of the $Fe(OH)_3^-$ ion are incorrect, but that magnetite phase stability probably shifts to favor a sodium ferric hydroxyphosphate compound in alkaline sodium phosphate solutions at elevated temperatures[4].

Our test methodology involved pumping alkaline solutions of known composition

through a bed of Fe_3O_4 granules and analyzing the emerging solution for Fe. Two pH-controlling reagents were tested: sodium phosphate and ammonia. Equilibria for the following reactions were described in thermodynamic terms: (a) $Fe(OH)_2/Fe_3O_4$ dissolution and transformation, (b) Fe(II) and Fe(III) ion hydroxocomplex formation (hydrolysis), (c) Fe(II) ion amminocomplex formation, and (d) Fe(II) and Fe(III) ion phosphatocomplex formation.

EXPERIMENTAL

Materials

Magnetite was prepared from reagent grade magnetite (Ferric-Ferrous Oxide, Black) supplied by Fisher Scientific Company. Because the as-received powder was too fine to be retained as a packed column in a flowing autoclave system, it was transformed into larger particles via the following operations: (1) pan-rolling into spheres by means of the snow-balling action provided in the catch pan of an automatic sieve; (2) hand sieving the spherical particles through a 10 mesh sieve onto a 20 mesh sieve; (3) firing for a minimum of two hours at 1400°C in a platinum dish (A 50/1 atmosphere of CO_2/CO gas was used to maintain the desired Fe(III)/Fe(II) ratio.); and (4) quenching in liquid nitrogen. The material produced in this manner consisted of shiny, hard, highly dense spheres having diameters between 0.6 and 1.2 mm. Density measurements using a mercury pycnometer gave a value of 4.59 gm/cm^3 (88% of theoretical), indicative of a high degree of sintering. Emission spectroscopic analysis found the following mass fractions of major impurities: 0.006 Mn, 0.0009 Mg, and 0.0005 Cr.

Examination of the magnetite spheres at high magnification by scanning electron

microscopy (SEM) revealed a relatively smooth surface composed of large, sintered grains (10 - 20 μm), see Fig. 1. X-ray diffraction analysis confirmed the presence of a single phase spinel-type oxide (lattice parameter = 8.4003 $\pm$0.0006 Å). Further characterization of the crystalline lattice configuration by Mössbauer spectroscopy indicated that the ratio of Fe(III)-Fe(II) ion pairs in octahedral sites (B) to Fe(III) ions in tetahedral (A) sites was 1.9 ($\pm$8%), a result consistent with the 2.0 value expected for a stoichiometrically pure magnetite lattice.

Deionized, deoxygenated water was used throughout the experimental program. This water had a resistivity $>$1 Mohm-cm and contained $<$0.1 mg/L silica. A commercial-grade nitrogen/hydrogen gas mixture was used to sparge dissolved oxygen to values $<$0.005 mg/L. Test solutions were prepared volumetrically in the feed tanks using reagent grade sodium phosphate and ammonium hydroxide.

Post-test SEM examination of the magnetite spheres after removal from the solubility apparatus revealed that a layer of fine ($<$1 μm) polyhedral crystals had formed on the smooth-grained surface during testing, see Fig. 1. This phenomenon is not unexpected and is related to 'outer layer' magnetite formation first observed by Potter and Mann[5] during the hydrothermal corrosion of iron. The actual process involves magnetite dissolution/recrystallization, in response to (undefined) electrochemical reactions with the liquid phase. The aqueous phase environment, i.e., solution chemistry and hydrodynamics, is known to affect size of the reprecipitated crystals[6]. Evidence of partial dissolution along selected crystal planes was also observed at 10,000X in a small number of the polyhedral microcrystals.

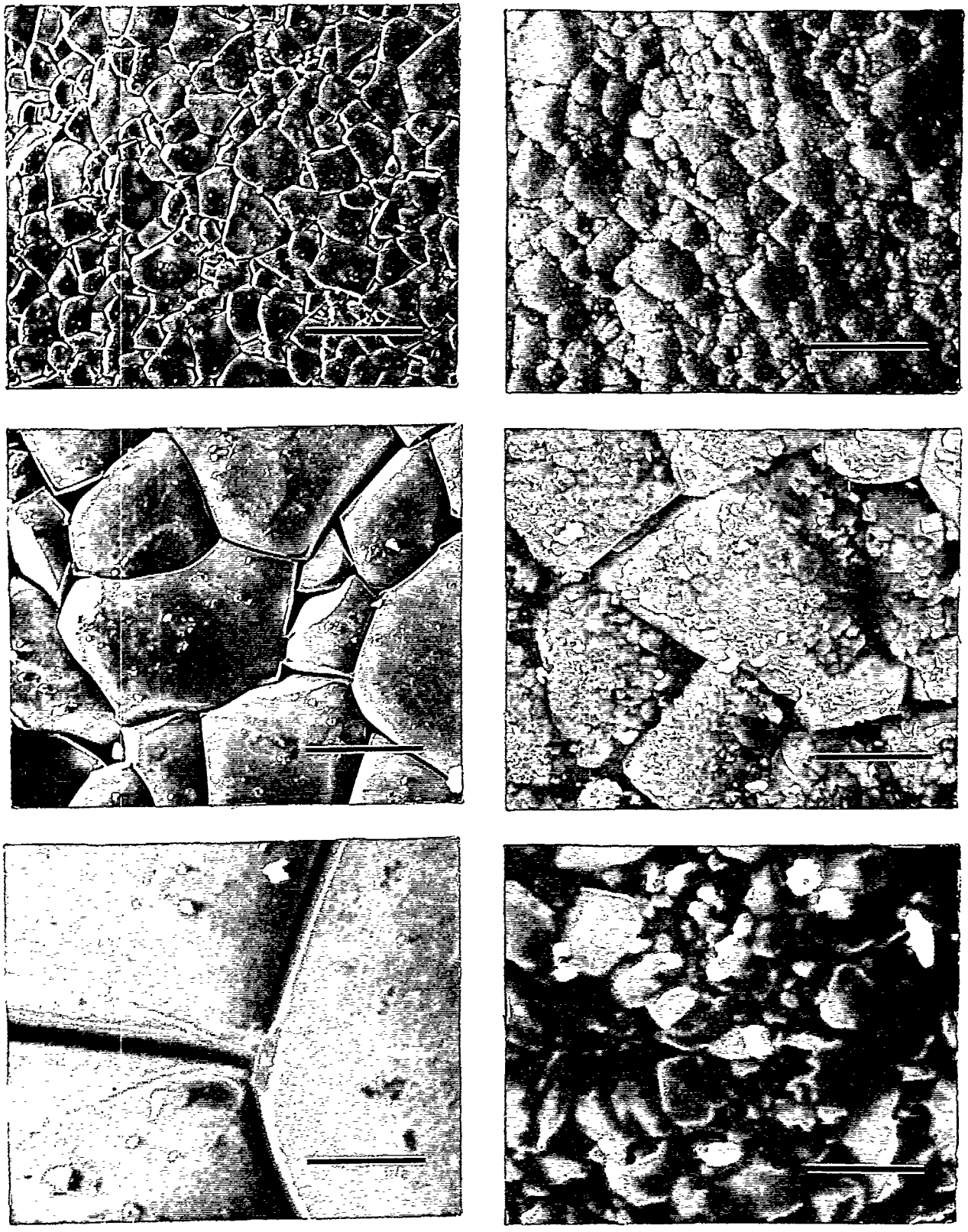

FIGURE 1 Scanning electron micrographs of magnetite (Fe_3O_4) surface: (a) as-sintered (left); (b) after solubility testing (right). Bar length corresponds to 40 μm, 10 μm and 2μm in respective top, middle, and bottom photographs

X-ray photoelectron spectroscopy (XPS) of the recrystallized, polyhedral magnetite crystals confirmed the presence of a submicroscopic hydrous iron oxide surface phase. Although deconvolution of iron oxide spectra in the Fe(2p) region is highly complex, the presence of a hydrous iron oxide phase was readily detected by detailed analyses of the O(1s) region. Figure 2 compares the O(1s) spectral lines observed for the pre- and post-test magnetite surfaces. These spectra illustrate that magnetite possesses a secondary peak centered 1.5 eV above the 529.5 eV primary O^{2-} peak. Similar behavior is observed for $NiFe_2O_4$[7], with the secondary peak (or high-binding energy tail) comprising nearly one-third of the total O(1s) peak area. Exposure to the test environment caused a major increase in the peak centered at 531 eV. This behavior is consistent with the presence of OH^- bonded oxygen, since the hydroxyl ion in α-FeOOH is known to produce a second O(1s) peak which occurs ~ 1.6 eV higher than the 529.8 eV peak for O^{2-} in α-Fe_2O_3[8]. The binding energy for this hydroxyl oxygen is nearly identical to that in $Ni(OH)_2$ and $Co(OH)_2$[8]. The decrease in intensity of the 531 eV peak after <100 Å of surface ion milling with argon indicates that the hydrous iron oxide phase is highly localized to the Fe_3O_4 surface.

Previous post-test surface characterization of magnetite after exposure in a similar solubility apparatus by X-ray photoelectron spectroscopy[2] revealed the presence of at least three to four monolayers of a hydrous Fe(II) oxide phase. Although it could not be concluded whether such a surface layer was present at equilibrium during the Reference 2 (high temperature) solubility measurements, this restriction does not apply in our case due to the extended temperature range of our study. We therefore conclude that such a surface layer also existed on our magnetite at low temperatures, and probably affected its solubility

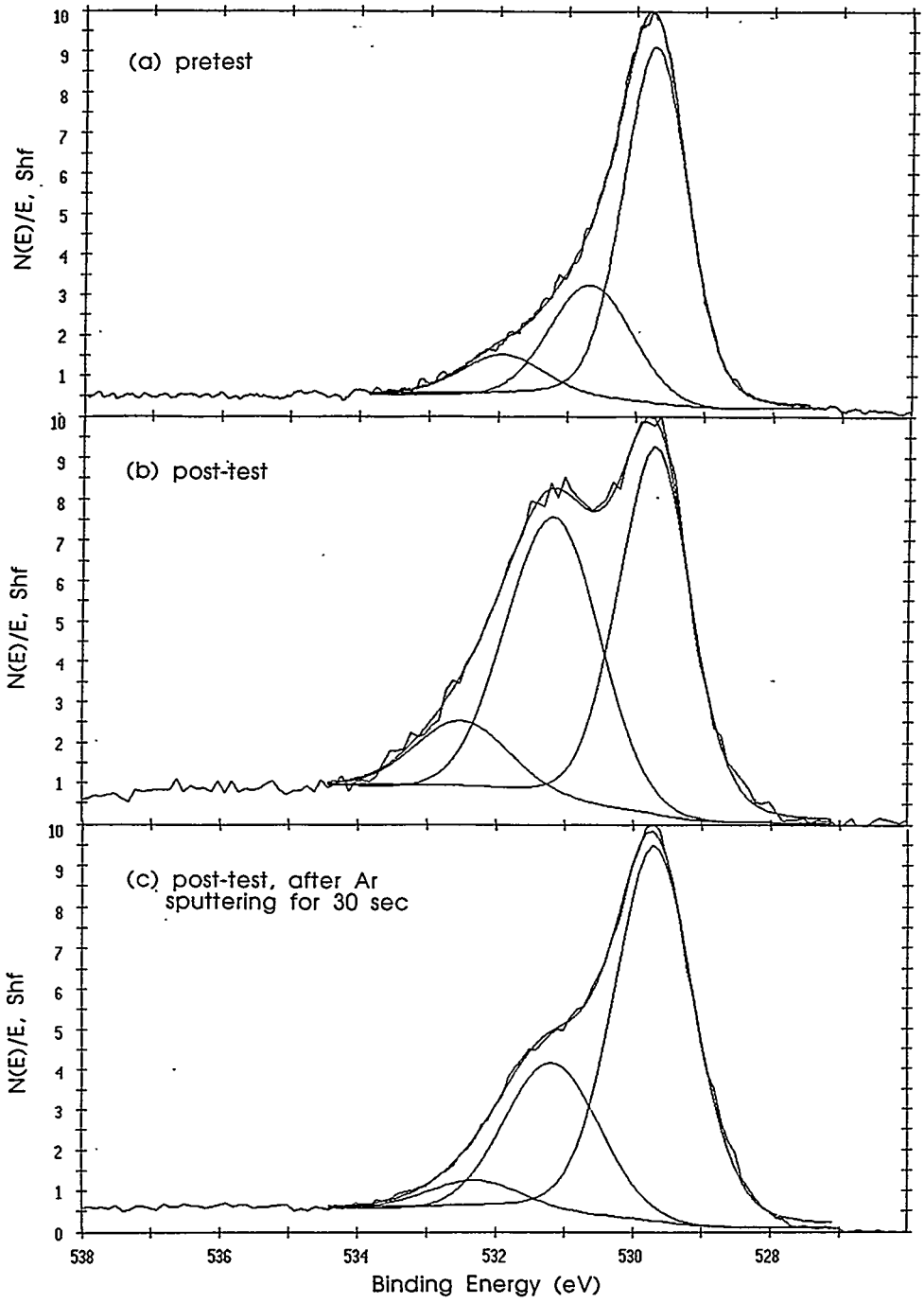

FIGURE 2 X-ray photoelectron O(1s) spectra of Fe_3O_4 surface: (a) pretest, (b) post-test, (c) post-test after Ar sputtering for 30 sec. The solid line drawn through the data is the sum of the individual band fits within the envelope. Note the appearance of a hydrous iron oxide surface phase (OH^- bond at 531 eV) upon exposure to the aqueous environment.

behavior in this temperature region.

Apparatus

The solubility measurements were made using two identical flowing autoclave systems. A diagram of an individual system is shown in Fig. 3. Although each system was constructed from stainless steel components, all high temperature portions, as well as the sampling lines, were platinum-lined. Further details on the construction and operation of the apparatus are described elsewhere[3]. The experimental program consisted of solubility measurements conducted in deoxygenated water maintained with a one atmosphere blanket of a nitrogen-hydrogen cover gas (30.5 vol% hydrogen, remainder nitrogen). The hydrogen concentration in the feedwater was calculated to be 5.3 $\pm$0.3 scm^3/kg, based on water temperature, cover gas composition, and Henry's law coefficient for the solubility of hydrogen in water. All feedwater compositions are shown in Table I. Run 9 was an abbreviated run in which the cover gas composition was changed to 100% hydrogen.

Maintenance of a flow rate of 5.5 $\pm$0.5 cm^3/min (at room temperature), together with a 260 g charge of magnetite, provided an average contact time between the feed solution and the iron oxide bed of 7 to 9 min, depending on the temperature. Preliminary experiments were conducted to determine whether solution flow rates through the bed had an affect on measured solubilities. These tests showed that there was no appreciable difference when the flow rate was varied from 3.15 to 15.4 cm^3/min. A flow rate of 5.5 $\pm$0.5 cm^3/min was chosen for use in the solubility program to provide a reasonable balance between time of contact with the magnetite bed, time of exposure to the sample cooler walls, and the capability of the system pump to maintain a constant, continuous flow.

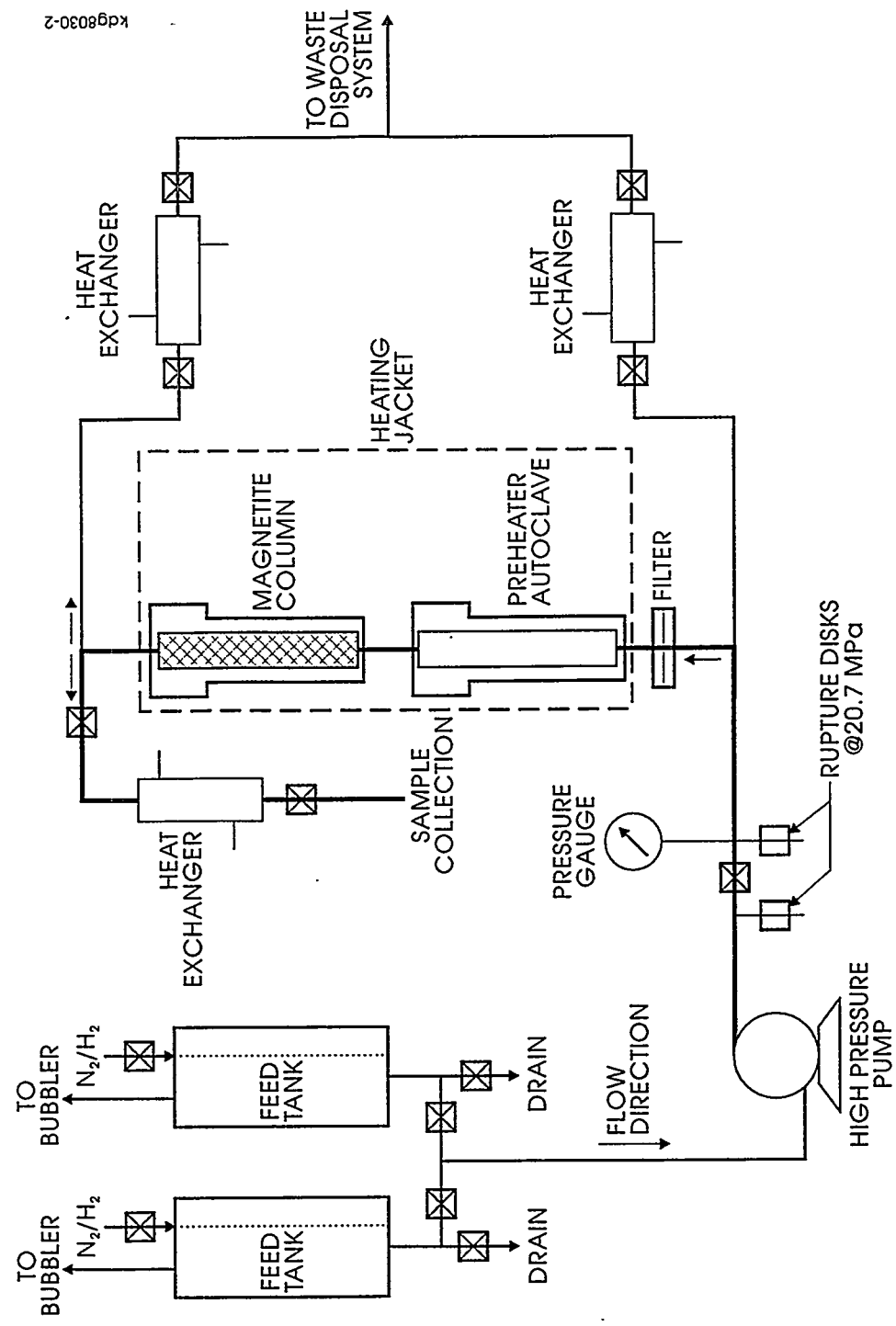

FIGURE 3 Schematic of flowing autoclave system used in magnetite solubility investigation

TABLE I. Feedwater Compositions*

Run	Phosphate, mmol/kg	Na/P, molar ratio	pH at 25°C	Conductivity, μS/cm
1	0.534 ± 0.014	2.297 ± 0.024	10.21 ± 0.01	141 ± 6
2	1.52 ± 0.06	2.339 ± 0.012	10.67 ± 0.02	410 ± 20
3	3.05 ± 0.03	2.358 ± 0.008	10.96 ± 0.02	802 ± 42
4	10.62 ± 0.02	2.314 ± 0.003	11.26 ± 0.01	2355 ± 14
5	53.3 ± 0.3	2.318 ± 0.003	11.34 ± 0.01	8585 ± 50
6	107.2 ± 0.3	2.294 ± 0.003	-	-
7	105.2 ± 0.5	2.143 ± 0.004	-	-
8	106.1 ± 0.5	2.787 ± 0.008	-	-
9	107.1 ± 1.3	2.300 ± 0.003	-	-
	Ammonia, mmol/kg			
10	0.079 ± 0.001		9.36 ± 0.08	6.7 ± 0.2
11	0.746 ± 0.018		10.05 ± 0.06	26.5 ± 0.5
11A	0.705 ± 0.018		10.14 ± 0.03	27.9 ± 0.6

*Dissolved hydrogen = 5.3 scm^3/kg (i.e., 237 μm) in all runs except Run 9 (17.7 scm^3/kg).

Operational and Analytical Procedures

After the system was stabilized at a desired temperature, steady-state conditions were maintained for at least sixty minutes; then flow was diverted into the sampling system. Six samples were collected at each temperature. Each sample, consisting of ~ 2 cm^3 of solution, was collected in a polystyrene atomic absorption autosampling vial containing 10 mm^3 of redistilled, concentrated nitric acid. After the six samples had been collected, the temperature controller and Variac settings were changed to establish a new temperature. From 30 to 90 min were required to stabilize the system at the new temperature. After an additional sixty minutes or longer, the sampling procedure was repeated. This process of changing temperature, allowing time for equilibration, and sampling, continued throughout each experimental run.

The samples were analyzed for iron by flameless atomic absorption techniques. A Perkin-Elmer Model 5000 Zeeman Atomic Absorption Spectrophotometer, equipped with a graphite furnace, was used for these analyses. A set of dilute nitric acid solutions containing known amounts of iron was run several times with each group of samples analyzed. The high sensitivity of this instrument eliminated the need for a preconcentration step, and allowed the iron analyses to be performed directly from the polystyrene vials in which the samples had been collected. Although direct analysis eliminated several sources of possible contamination, it also presented a new problem: despite visual screening of the vials to eliminate those with black specks imbedded in the plastic (possible sources of iron contamination), and acid leaching those that passed inspection, it was found that the iron concentration in samples stored in the vials for a period of 5 hr increased by approximately

0.009 μm, and after two days had increased by about 0.036 μm. Fortunately, this phenomenon was discovered during the preliminary, shakedown phase, so that all reported iron analyses represent those analyzed immediately (i.e., <3 hr) after they were collected. It is estimated that the iron analyses had an accuracy of $\pm$5%.

Ammonia concentrations were determined in feedwater, and in some effluent samples, using standard colorimetric procedures. A Perkin-Elmer Lambda 3 UV-VIS Spectrophotometer was used for these analyses. Phosphate concentrations and sodium-to-phosphate molar ratios were determined by potentiometric titration with dilute hydrochloric acid[4].

The actual experimental program consisted of 11 nominal runs (Table I) during which a temperature range of 21 to 288°C was covered. In two of the initial runs (Runs 10 and 11), approximately one-half of the samples were taken during an ascending sequence of temperature changes, the remaining half during a descending sequence of changes. A small hysteresis, or memory effect, was observed in some of the measured solubilities at temperatures below 121°C after the system had been operated at 288°C, and above 121°C after prior operation at lower temperatures. As a result of this testing, the subsequent sampling/operating sequence was modified to include two temperature sequences: one between 21 and 135°C (ascending) and one between 288 and 121°C (descending/ascending). To allow time for oxide transformation into the stable low/high temperature form, the bed was operated for 6 days at room temperature, or for 2 days at 260°C, prior to initiating the respective low and high temperature sampling sequences.

RESULTS

Solubility Data

Results from the experimental program, in terms of measured iron solubilities as a function of temperature, are presented in Table II. The elemental iron concentrations represent averages of six samples and are given in micromolality units (μm, micromoles of iron per kilogram of water). Scatter about the reported means was $\pm 6\%$. The small amounts of material lost in the sampling line have been neglected: acid cleaning of the sampling line/cooler upon completion of the experimental program revealed only trace accumulations of iron. The temperature value listed for an individual sample was the average of the two downstream thermocouple readings at the start and completion of sampling. Temperature stability within $\pm 0.5°C$ was achieved during collection of all samples.

It is estimated that the overall accuracy of the solubility measurements, including system effects and measurement errors, was $\pm 20\%$ (1σ), based on the observed deviations between Run 11 and its replicate. This estimate is probably conservative because Run 11 also had the lowest measured iron concentrations.

Thermodynamic Analysis

Magnetite is expected to solubilize in high temperature aqueous solutions via the Eqs. (1, 2) reaction sequences. At lower temperatures, where a layer of hydrous Fe(II) oxide, i.e., $Fe(OH)_2(s)$, is expected to exist on the magnetite surface, the applicable solubilization reaction sequence is

$$Fe(OH)_2(s) + (2-n)H^+ \rightleftharpoons Fe(OH)_n^{2-n} + (2-n)H_2O \qquad (4)$$

where n has the same range as in Eq. (1). An analogous reaction sequence exists for the

TABLE II. Measured Solubilities of Magnetite in Aqueous Solutions

Fe[a]	T(K)	Fe[a]	T(K)	Fe[a]	T(K)	Fe[a]	T(K)
Run 1		Run 2		Run 3		Run 4	
0.0510	294.8	0.0544	294.3	0.0362	295.9	0.0673	295.9
0.0417	311.5	0.0451	294.8	0.0437	310.9	0.0525	311.5
0.0451	325.9	0.0550	310.4	0.0383	324.3	0.0543	324.3
0.0634	337.6	0.0476	311.5	0.0430	338.2	0.0457	340.4
0.0675	352.0	0.0580	323.7	0.0358	351.5	0.0403	352.6
0.0686	352.6	0.0659	324.3	0.0539	352.0	0.0612	394.8
0.0666	365.9	0.0623	337.0	0.0509	366.5	0.0587	408.2
0.0564	380.4	0.0840	338.7	0.0539	381.5	0.0748	423.7
0.0475	381.5	0.0688	352.0	0.0550	393.7	0.1005	435.9
0.0535	394.8	0.0788	353.7	0.0559	408.7	0.0933	450.4
0.0448	395.4	0.0800	365.9	0.0544	409.3	0.1189	463.2
0.0537	408.7	0.0596	381.5	0.0634	421.5	0.1492	479.3
0.0492	423.2	0.0500	396.5	0.0571	424.8	0.2364	492.6
0.0496	435.4	0.0559	410.9	0.0630	435.9	0.2614	504.8
0.0505	436.5	0.0650	422.0	0.0743	450.9	0.3868	518.2
0.0639	449.3	0.0603	423.7	0.0949	464.3	0.5712	532.0
0.0630	462.0	0.0661	434.3	0.0994	477.0	0.8487	545.9
0.0729	477.0	0.0725	439.3	0.1252	490.9	1.148	560.9
0.0736	492.0	0.0813	452.6	0.2238	519.8		
0.0859	504.3	0.0859	466.5	0.3545	532.6		
0.0944	518.7	0.0988	479.8	0.3116	533.2		
0.1282	533.2	0.1094	489.8	0.4411	547.6		
0.1526	533.7	0.1323	505.4	0.5336	559.8		
0.1549	547.0	0.1608	520.4				
0.1764	560.4	0.2095	532.0				
0.1982	560.9	0.2471	534.3				
		0.2722	545.9				
		0.2865	546.5				
		0.3366	559.8				
		0.3527	560.4				
Run 5		Run 6		Run 7		Run 8	
0.2829	295.4	1.1764	298.2	0.7574	297.6	0.5515	300.9
0.1952	310.9	0.8864	310.4	0.6697	310.4	0.6052	310.9
0.1809	323.7	0.6589	324.8	0.4566	324.3	0.5300	322.6
0.1194	339.8	0.4405	338.2	0.2972	339.8	0.5014	335.9
0.1155	352.0	0.4100	350.9	0.3205	350.9	0.2578	350.4
0.1074	364.3	0.3707	367.6	0.3080	365.9	0.5605	394.8
0.1826	393.2	0.3259	409.8	0.2185	408.2	0.6572	407.0
0.2668	409.3	0.5139	424.3	0.3295	424.8	1.056	420.9
0.3653	423.7	0.6554	436.5	0.3957	435.9	1.101	422.0
0.4262	435.4	0.8452	450.9	0.4817	450.4	1.723	437.6
0.6482	453.7	1.0869	464.3	0.6034	463.7	2.793	460.4
0.8667	464.3	1.7888	479.3	0.8595	479.3	6.482	490.4
1.232	478.7	1.916	492.0	1.687	507.6	10.06	524.3
1.395	490.4	3.438	507.0	2.256	516.5	15.13	534.3
1.311	503.7	4.441	517.0	3.742	530.9	21.72	547.0
1.934	517.6	7.377	530.9	5.873	546.5	27.27	560.4
3.528	534.8	10.21	545.9	8.523	562.0		
3.832	543.7	14.83	562.0				
5.533	559.3						
Run 9		Run 10		Run 11		Run 11A	
0.7682	300.9	0.0483	297.0	0.0313	312.6	0.0204	294.8
0.6178	311.5	0.0548	313.2	0.0329	324.8	0.0206	310.4
0.5336	323.2	0.0573	326.5	0.0265	338.2	0.0313	324.3
0.4208	335.4	0.0627	339.3	0.0351	351.5	0.0322	337.0
0.1791	350.9	0.0985	353.2	0.0337	365.4	0.0349	355.4
0.1719	365.9	0.0949	364.8	0.0294	395.4	0.0417	367.0
0.2274	381.5	0.0859	379.8	0.0374	408.2	0.0353	380.4
0.2775	393.2	0.0824	394.8	0.0286	419.8	0.0346	394.8
0.3259	407.0	0.0877	409.3	0.0390	435.4	0.0285	407.0
0.4190	421.5	0.0716	421.5	0.0372	450.9	0.0283	420.4
0.4530	423.2	0.0716	437.6	0.0401	464.8	0.0322	434.3
5.103	531.5	0.0537	452.6	0.0405	478.7	0.0281	447.6
5.336	532.0	0.0573	464.3	0.0417	491.5	0.0301	462.6
6.769	545.9	0.0501	478.2	0.0349	505.4	0.0356	478.2
8.326	560.4	0.0537	492.0	0.0421	519.3	0.0333	490.4
		0.0466	505.4	0.0331	532.0	0.0317	504.3
		0.0537	518.7	0.0324	547.0	0.0283	505.9
		0.0466	532.6			0.0258	519.3
		0.0483	533.7			0.0270	532.0
		0.0483	548.2			0.0274	546.5
		0.0501	560.4			0.0340	547.0
						0.0312	559.8
						0.0267	560.9

[a]Units: 10^{-6} mol-kg water^{-1}.

oxidative dissolution of hydrous Fe(II) oxide into Fe(III) ion hydroxocomplexes.

In aqueous solutions containing other dissolved species, such as those introduced via the pH-determining reagents, other types of Fe(II) and Fe(III) ion complexes are possible. For example, phosphatocomplexes of the unhydrolyzed Fe(II) and Fe(III) ions with both the $HPO_4^=$ and $H_2PO_4^-$ ions have been reported[9, 10], and multiple, hydrolyzed forms, such as $Fe(OH)_m(HPO_4)_p^{(3-m-2p)+}$, $Fe(OH)_m(H_2PO_4)_q^{(3-m-q)+}$, and $Fe(OH)_n(HPO_4)_r^{(2-n-2r)+}$ are possible in alkaline solutions. In addition, the following Fe(II)-ammonia complexes are known to exist: $Fe(NH_3)_a^{2+}$ (a = 1, 2)[11] and mixed hydroxoamminocomplexes, such as $Fe(OH)_n(NH_3)_a^{(2-n)+}$ (n = 1, 2, 3), are possible in alkaline solutions.

By expressing the concentration of each possible Fe(II) and Fe(III) ion complex in terms of an equilibrium constant and calculable H^+, $H_2PO_4^-$, and HPO_4^{2-} ion concentrations, the measured iron ion solubilities were separated into contributions from each of the individual complexes. The thermodynamic relationships

$$-RT\ln K = \Delta G = \Delta H - T\Delta S \tag{5}$$

were introduced at this point to permit calculation of all iron ion complex concentrations as functions of temperature. Where possible, a three parameter model was used to describe $\Delta G(T)$. This approximation assumes that the difference in heat capacities between reactants and products for each reaction is a constant (C). Integration of the applicable thermodynamic relationships gives

$$\Delta G(T) = A - BT - CT\ln T \tag{5a}$$

where the constants A, B, and C have the thermodynamic significance:

$A = \Delta H(298) - 298\Delta C_p$

$B = \Delta S(298) - (1 + \ln 298)\Delta C_p$

$C = \Delta C_p$

The total molality of iron ions in solution was then calculable by summation over all mononuclear iron ion species present.

To evaluate the experimental solubilities of Table II in terms of concentrations of the possible hydrolyzed/complexed iron ion species present required that the pH (hydronium ion concentration) be known at the existing solution conditions. This quantity depended on the molality of the alkaline reagents dissolved in solution (i.e., sodium phosphate or ammonium hydroxide), as well as their dissociation constants and that of H_2O. The latter parameters, which are functions of solution temperature, are defined below in terms of thermodynamic activities ( ) and tabulated in Table III.

$$K_w = (H^+)\,(OH^-) \tag{6}$$

$$K_B = (NH_4^+)(OH^-) \;/\; (NH_3) \tag{7}$$

$$K_1 = (H_2PO_4^-) \;/\; (H_3PO_4)(OH^-) \tag{8}$$

$$K_2 = (HPO_4^{2-}) \;/\; (H_2PO_4^-)(OH^-) \tag{8a}$$

$$K_3 = (PO_4^{3-}) \;/\; (HPO_4^{2-})(OH^-) \tag{8b}$$

$$with\ \log K = b_1/T + b_2 + b_3 \ln T + b_4 T + b_5/T^2 \tag{9}$$

In addition, the equivalent pressure of hydrogen dissolved in water at 25°C (P_o =

TABLE III. Dissociation Behavior of Selected Compounds*

Compound Undergoing Dissociation	b_1	b_2	b_3	b_4	b_5	Reference Cited
H_2O	31,286.0	-606.522	94.9734	-0.097611	-2,170,870	Sweeton, Mesmer and Baes[12]
NH_3	27,496.7	-513.761	81.2824	-0.0905795	-1,717,720	Hitch and Mesmer[13]
H_3PO_4	17,655.8	-253.198	39.4277	-0.0325405	-810,134	Mesmer and Baes[14]
$H_2PO_4^-$	17,156.9	-246.045	37.7345	-0.0322082	-897,579	Mesmer and Baes[14]
HPO_4^{2-}	-106.51	7.1340	-	-0.017459	-	Treloar[15]
H_2 (Henry's Law)	27,416.5	-449.429	70.6703	-0.0655463	-1,848,130	Gilpatrick and Stone[16]

*Via Eq. (9)

0.305 atm) was calculated as a function of temperature by application of Henry's law; i.e., $PH_2(T) = (H(T)/H_o)\, P_o$. For thermodynamic consistency, values for Henry's law constant, H(T), were calculated using the data of Gilpatrick and Stone[16] fitted to Eq. (9) with log K replaced by log H (atm/mol fraction).

Deviations from ideal solution behavior were negligible in Runs 1, 10, and 11 where ionic strengths were on the order of 10^{-3} or less. However, in Runs 2 to 9, phosphate concentrations approached 0.1 m and it became necessary to account for small deviations from ideality. Such deviations were accounted for by distinguishing between ionic concentration and thermodynamic activity:

$$(a_i) = \gamma_i[C_i] \tag{10}$$

where (a_i) is the thermodynamic activity, γ_i the ionic activity, and $[C_i]$ is the ionic concentration. Generally it was assumed that ionic activity was related to ionic strength by an extended Debye-Hückel expression[17]:

$$\log\gamma_i = -SZ_i^2\sqrt{I}/(1 + 1.5\sqrt{I}) \tag{11}$$

where S is the temperature-dependent[17], limiting Debye-Hückel slope (= 0.51 at 298 K), Z_i is the ionic charge number, and I is the ionic strength ($= \frac{1}{2}\Sigma C_i Z_i^2$). Dissociation constants K_1 and K_2 were corrected for ionic strength via literature correlations[14], while K_w and K_B were pressure corrected (to 8.97 MPa) as well as ionic strength corrected using the correlations developed in References [12] and [13].

An overall electroneutrality balance was finally applied to determine $[H^+]$ for each data point. For the most general case, with sodium phosphate and ammonia present, the

balance is:

$$[Na^+] + [NH_4^+] + [H^+] + \sum_{k=0}^{2}\sum_{n=0}^{3}(2-n)\left[Fe(OH)_n(NH_3)_k^{(2-n)+}\right]$$

$$+\sum_{m=3}^{4}(3-m)\left[Fe(OH)_m^{(3-m)+}\right] + \sum_{p=1}^{2}\sum_{n=1}^{3}(2-n-2p)\left[Fe(OH)_n(HPO_4)_p^{(2-n-2p)+}\right]$$

$$+\sum_{r=1}^{2}\sum_{n=1}^{3}(2-n-r)\left[Fe(OH)_n(H_2PO_4)_r^{(2-n-r)+}\right] + \sum_{s=1}^{2}\sum_{m=3}^{4}(3-m-2s)\left[Fe(OH)_m(HPO_4)_s^{(3-m-2s)+}\right] \quad (12)$$

$$+\sum_{t=1}^{3}\sum_{m=3}^{4}(3-m-t)\left[Fe(OH)_m(H_2PO_4)_t^{(3-m-t)+}\right] = [OH^-] + 3[PO_4^{3-}] + 2[HPO_4^{2-}] + [H_2PO_4^-]$$

Since all terms were expressible in terms of temperature, total dissolved ammonia, and phosphate concentration (and sodium-to-phosphate ratio), the neutrality balance was reduced to an algebraic equation in terms of the unknown, $[H^+]$. To determine how a given scheme of iron ion complexes in solution could fit the results, a set of thermodynamic constants was substituted into the neutrality balance, Eq. (12), and $[H^+]$ concentrations were calculated by a Newton-Raphson iteration procedure. These $[H^+]$ values were then used to compute all the soluble iron ion species which, after being summed, could be compared with the measured iron solubilities. The differences were then minimized via a generalized, nonlinear, least-squares curve-fitting routine based on Marquardt's algorithm[18].

When the solubility data were analyzed, the importance of relative errors (i.e., percentage errors), rather than absolute errors, was accounted for by minimizing differences between the logarithms of the experimental and the predicted solubilities. The thermodynamic functions obtained in this manner were then resubstituted into the neutrality balance, and the two-step process was repeated. Convergence, i.e., the condition when the

calculated thermodynamic functions ceased to change, was attained after a few cycles because the dissolved metal cationic complexes were very low and had only a minor influence on changes in solution pH. When it became apparent that a possible magnetite solid phase transformation was occurring, an additional type of iteration was performed. Using an initial estimate of 120°C for the suspected $Fe_3O_4/Fe(OH)_2$ transformation, a new estimate for the transformation temperature was obtained based on the fitted free energies of the two dissolution reactions, i.e., the n = 0 form of Eqs. (1, 4). The least-squares fitting procedure using the revised transformation temperature was then repeated until the estimated and calculated values agreed. Note that a higher transformation temperature is required for Run 9 due to the higher level of dissolved hydrogen (see DISCUSSION).

Practical considerations limited our database to an alkaline pH region, and only one (partial) run was performed in which a second level of dissolved hydrogen was used. Therefore, it was not possible to simultaneously fit all the thermodynamic parameters for the entire set of Fe(II) and Fe(III) complexes and a number of constraints was placed on the fit. Each of these constraints was made to insure consistency with previously-accepted, reliable results.

To compensate for the insignificant concentrations of Fe(II) and Fe(III) anionic hydroxocomplexes expected to be present at low temperatures, $\Delta G°(298)$ values for their formation via hydrolysis, i.e.

$$Fe(OH)_2(aq) + H_2O \rightleftharpoons Fe(OH)_3^- + H^+ \qquad (13)$$

and

$$Fe(OH)_3(aq) + H_2O \rightleftharpoons Fe(OH)_4^- + H^+ \quad (14)$$

were obtained by employing two constraints derived from available literature. The recommended value for Eq. (14) is 54.81 kJ/mol[19]. On the other hand, the Baes and Mesmer-recommended value for Eq. (13) has been rejected on the basis that it was derived from an analysis of magnetite solubility data that neglected the contribution of Eqs. (3, 14). By accounting for this effect, Tremaine and LeBlanc[2] demonstrated that a higher ΔG° value is required for Eq. (13), which is also compatible with those observed for Ni(II)[3] and Co(II)[20]. We, therefore, employed an indirect constraint on ΔG° for Eq. (13); namely, constraining ΔG° for Eq. (3). In doing so, we detected a minor inconsistency in the analysis of Tremaine and LeBlanc, since the literature basis for the Fe^{2+}/Fe^{3+} redox reaction at room temperature was not entirely recognized: the results of Larson et al.[21] and Wagman et al.[22] consistently recommend $\Delta G^\circ(298) = 74.3$ kJ/mol. Using the Baes and Mesmer compilation of hydrolytic equilibria[19] for $Fe(OH)_2(aq)$ and $Fe(OH)_3(aq)$ formation, together with the above Fe^{2+}/Fe^{3+} redox equilibrium, $\Delta G^\circ(298) = 25.4$ kJ/mol is derived for Eq. (3), rather than the Tremaine and LeBlanc estimate of 18.0 kJ/mol.

Two additional constraints were required to counteract a limited redox database. Consistent with the previously observed effects of dissolved hydrogen on magnetite solubility at 300°C[2], $\Delta G(573\ K)$ for Eq. (3) was constrained to the value 8.15 kJ/mol[2]. Similarly, the redox equilibrium involving the anionic hydroxocomplexes

$$Fe(OH)_3^- + H_2O \rightleftharpoons Fe(OH)_4^- + \tfrac{1}{2}H_2(g) \quad (15)$$

was constrained to 0.72 kJ/mol at 573 K[2]. These constraints provided concentration ratios

of Fe(III)/Fe(II) species of 3/7 and 2/1 in the respective Eqs. (3, 15) at 300°C for a dissolved hydrogen concentration of 779 μm.

In recognition of the above phenomena, two databases were constructed for least-squares analysis. The first consisted of data from Runs 10 and 11/11A (in ammonium hydroxide) and included the Fe_3O_4 solubility data in sodium hydroxide reported by Tremaine and LeBlanc[2] for $[Na^+] > 3.7$ μm and $T > 150$°C. This fit served as a consistency check for the $Fe(OH)^+$ species and allowed independent determination of reaction equilibria for amminocomplexing and hydrous Fe(II) oxide dissolution. The second database consisted of the first plus the remaining data from Table II, i.e., Runs 1 - 9.

Results of the least-squares fit of the magnetite solubility database in ammonium and sodium hydroxide are illustrated in Figs. 4 and 5 using a three-parameter thermodynamic model to describe the Eq. (1) magnetite dissolution equilibrium for $n = 0$ and a two-parameter model, i.e., $\Delta C_p = 0$ in Eq. (5), to describe the remaining hydrolysis and oxidation reaction equilibria. We found it necessary to account for the existence of a hydrous Fe(II) oxide phase at $T \leq 83$°C and to include a mixed hydroxoamminocomplex of the Fe(II) ion: $Fe(OH)(NH_3)^+$. All fitted thermodynamic quantities for the $Fe_3O_4/Fe(OH)_2$ dissolution reaction(s) and the subsequent Fe(II) ion hydrolysis, oxidation, and amminocomplexing reactions are summarized in Table IV. This fit produced an overall standard deviation between measured and fitted Fe solubilities of $\pm 19\%$; the Tremaine and LeBlanc data gave $1\sigma = \pm 28\%$ while Runs 10, 11/11A gave $1\sigma = \pm 14\%$. This agreement is considered consistent with the stated accuracy of the experimental measurements. Note that the four constraints employed to fit three iron ion hydrolysis/oxidation equilibria, i.e., Eqs. (3, 13,

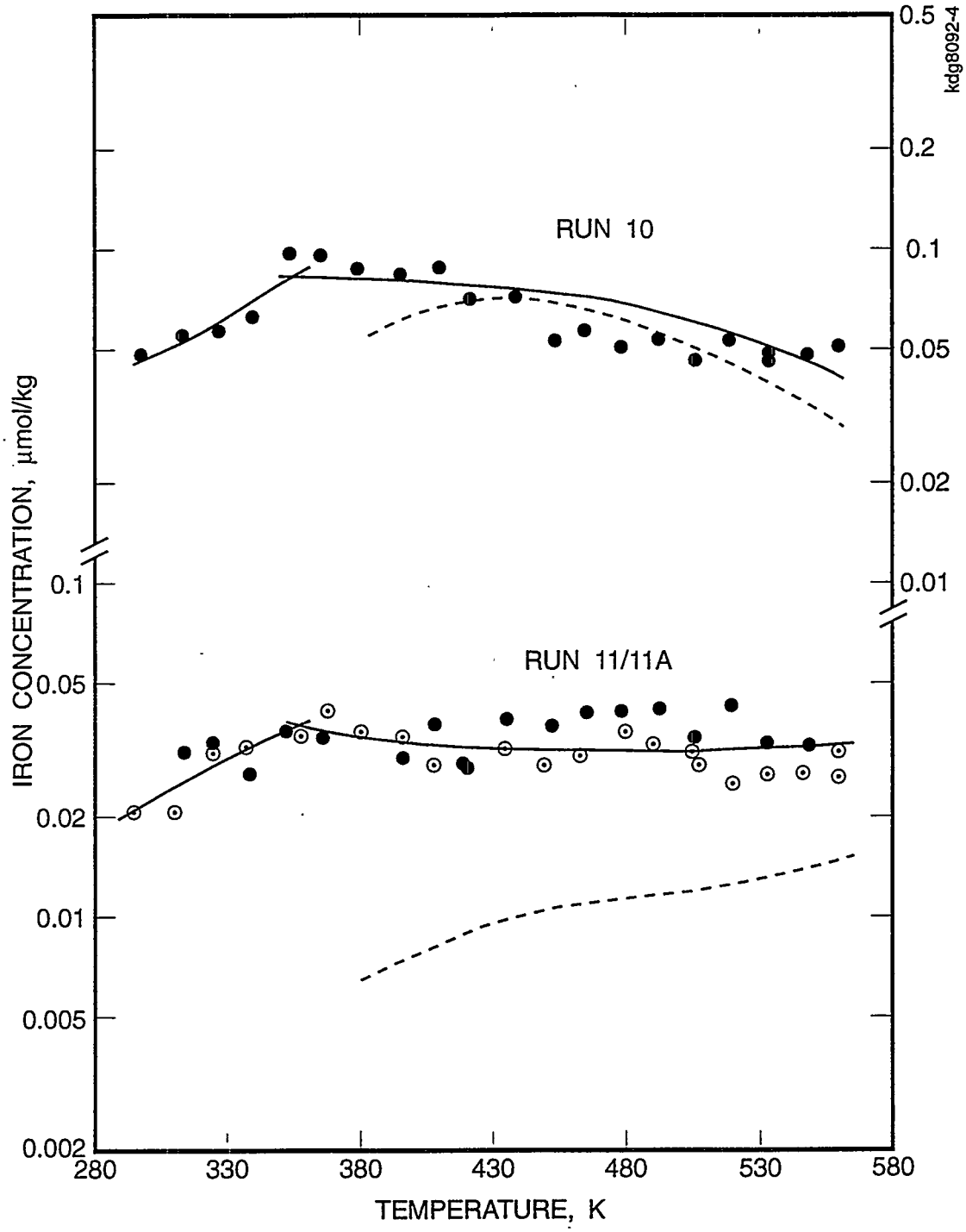

FIGURE 4 Comparison of measured and fitted solubilities of magnetite in ammonium hydroxide solutions. Dashed lines represent predicted magnetite solubilities based on results of Tremaine and LeBlanc[2], where amminocomplexing is excluded.

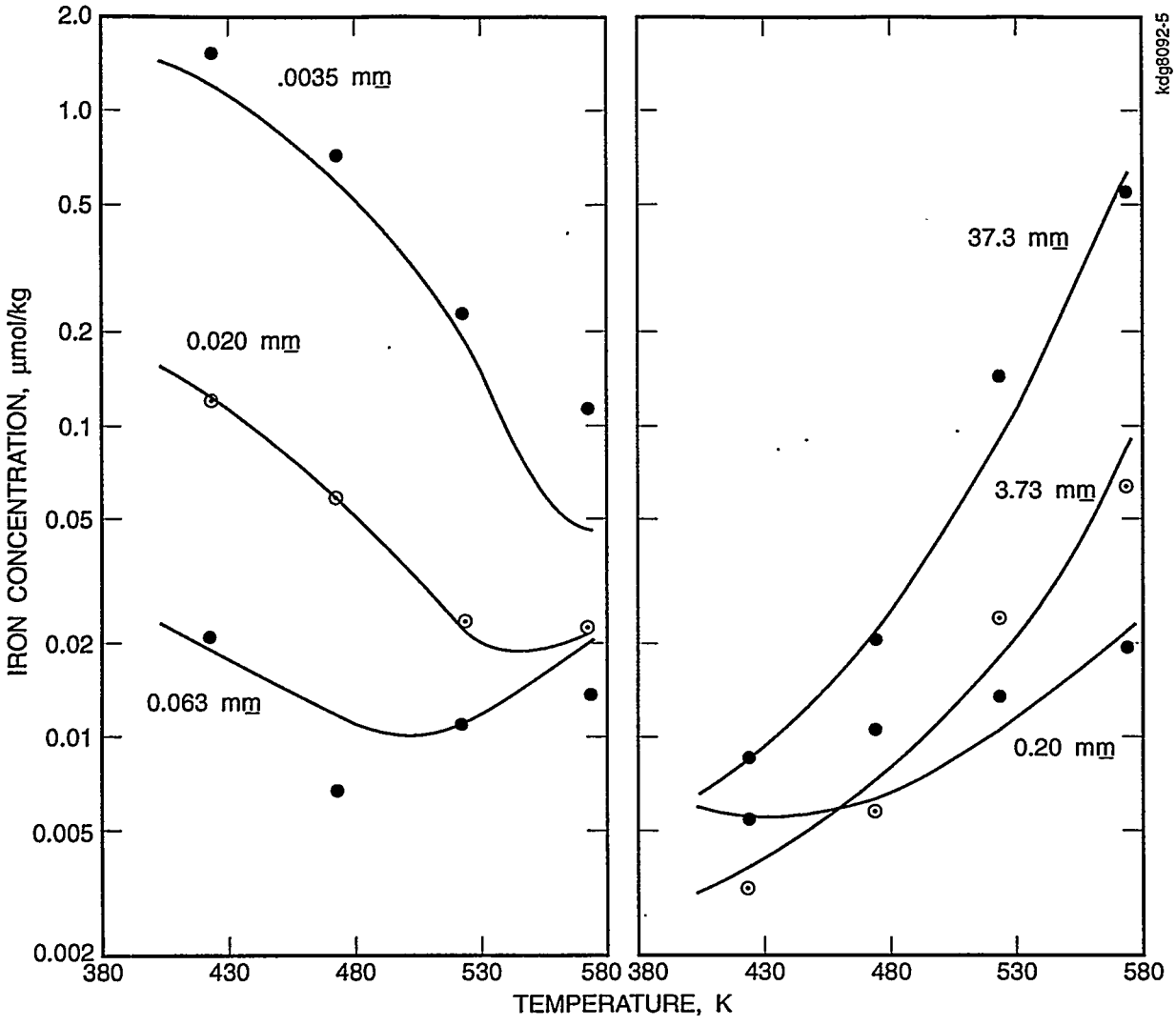

FIGURE 5 Comparison of measured and fitted solubilities of magnetite in sodium hydroxide solutions: (a) [NaOH] < 0.07 mm; (b) [NaOH] > 0.2 mm. Data taken from Tremaine and LeBlanc[2].

TABLE IV

Thermodynamic Parameters for the Calculation of Magnetite Solubilities in Ammonium and Sodium Hydroxide Solutions*

Reaction	A, kJ/mol	B, J/mol-K	C, J/mol-K	$\Delta G°(298)$, kJ/mol
		Dissolution		
$Fe(OH)_2(s) + 2H^+ \rightleftarrows Fe^{2+} + 2H_2O$	-76.96 ± 9.16	-49.34 ± 24.74	-	-62.25 ± 1.90
$⅓Fe_3O_4(s) + 2H^+ + ⅓H_2(g) \rightleftarrows Fe^{2+} + 4/3H_2O$	-136.15 ± 18.30	-983.68 ± 281.46	131.30 ± 39.44	-65.90 ± 1.54
		Hydrolysis		
$Fe^{2+} + H_2O \rightleftarrows Fe(OH)^+ + H^+$	19.68 ± 12.18	-105.33 ± 34.92	-	51.08 ± 2.96
$Fe^{2+} + 2H_2O \rightleftarrows Fe(OH)_2(aq) + 2H^+$	97.26 ± 4.87	-63.76 ± 9.94	-	116.27 ± 1.95
$Fe(OH)_2(aq) + H_2O \rightleftarrows Fe(OH)_3^- + H^+$	42.51 ± 9.55	(-91.63)**	-	69.83
$Fe(OH)_3(aq) + H_2O \rightleftarrows Fe(OH)_4^- + H^+$	19.18 ± 1.04	(-119.35)**	-	54.77
		Oxidation		
$Fe(OH)_2(aq) + H_2O \rightleftarrows Fe(OH)_3(aq) + ½H_2(g)$	(44.10)**	(62.72)**	-	25.40
		Amminocomplexing		
$Fe^{2+} + NH_3(aq) \rightleftarrows Fe(NH_3)^{2+}$	(-11.18 ± 0.56)[23]	(2.54 ± 5.06)[23]	-	(-11.93 ± 0.95) [23]
$Fe(OH)^+ + NH_3(aq) \rightleftarrows Fe(OH)(NH_3)^+$	18.52 ± 10.54	125.32 ± 30.67	-	-18.84 ± 2.30

* Via $\Delta G = A - BT - CT \ln T$. All reported uncertainties correspond to one standard deviation. **Notes: (a) Eq. (3) equilibrium fixed using constraints at 298 and 573 K, as discussed in text; (b) ΔS° for Eq. (14) calculated from constrained ΔG° and fitted ΔH_{14}; (c) ΔS° for Eq. (13) calculated from constraint derived in text using ΔHs for Eqs. (13, 14): $\Delta S_{13} = (\Delta H_{13} + 0.9224\ \Delta H_{14} - 112{,}725)/573.15$.

14), required that only two of six model parameters be fitted by the least-squares analysis.

The philosophy employed during analysis of the second database recognized HPO_4^{2-} as the preferred hydrolytic state of the orthophosphate ion in our range of Na/P ratios and temperatures. Therefore, this species was selected as the most probable ligand for complexing the soluble Fe(II) and Fe(III) hydroxocomplexes. Due to the demonstrated dominance of the n=1, 2, and 3 Fe(II) hydroxocomplexes over those of their Fe(III) counterparts in the low temperature region, only Fe(II) phosphatocomplexes were fitted in this region. Then, because the m=3 and 4 Fe(III) hydroxocomplexes increased in importance relative to their n=2 and 3 Fe(II) counterparts at high temperature/pH, their phosphatocomplexes with HPO_4^{2-} were given preference. Finally, to allow for the increased significance of the $H_2PO_4^-$ hydrolytic species in our solutions at elevated temperatures, additional $H_2PO_4^-$ phosphatocomplexes with the n=2 and 3 Fe(II) and m=3 and 4 Fe(III) hydroxocomplexes were attempted.

Special precautions were taken when fitting the $H_2PO_4^-$ ion complexing equilibria, since consistency with two additional equilibria needed to be demonstrated. That is, formation of the $Fe(OH)_2(H_2PO_4)^-$ species needed to consider the $Fe(OH)(HPO_4)^-$ formation reaction, since the two species differ by only a complexed water molecule:

$$Fe(OH)(HPO_4)^- + H_2O \rightleftharpoons Fe(OH)_2(H_2PO_4)^- \qquad (16)$$

Therefore, the two species could not be fitted simultaneously (for a given data point). However, by recognizing that the above transformation is temperature dependent, $Fe(OH)_2(H_2PO_4)^-$ concentrations were calculated at temperatures below the Eq. (16) transformation from a fit of the $Fe(OH)(HPO_4)^-$ species by applying the Eq. (16) equilibrium.

Similarly, $Fe(OH)(HPO_4)^-$ concentrations were calculated above the transformation temperature from a fit of the $Fe(OH)_2(H_2PO_4)^-$ species by invoking the Eq. (16) equilibrium. The other equilibrium to be considered was related to Fe(II) ion oxidation and the overlapping solubility domains of $Fe(OH)_2(H_2PO_4)^-$ and $Fe(OH)_3(H_2PO_4)^-$:

$$Fe(OH)_2(H_2PO_4)^- + H_2O \rightleftharpoons Fe(OH)_3(H_2PO_4)^- + \tfrac{1}{2}H_2(g) \qquad (17)$$

Due to the inadequacy of our redox database, the entropy change for Eq. (17) was constrained to that found for Eq. (3), see Table IV. The assumption that Fe(II) ion oxidation is unaffected by phosphato-complexing is justified as a first order approximation since the charge on the $H_2PO_4^-$ ligand is the same as that of the OH^- ion and it will be shown (Fig. 15) that hydrolysis does not appreciably affect ΔS of the ferrous ion oxidation reaction equilibria.

Results of the least-squares fit of the second database are illustrated in Figs. 6 through 9. Note that some of the solubility data recorded from runs at the highest phosphate concentrations (i.e., >50 mm) exhibited systematic deviations with respect to the assumed stability of the anhydrous and hydrous oxide phases. These regions of deviation were refitted to be consistent with a delayed dehydration/hydration reaction (see dashed lines). We judge the best fit of the data to be the following phosphatocomplexing scheme:

low temperature forms: $Fe(OH)(HPO_4)^-$, $Fe(OH)_2(HPO_4)^{2-}$, and $Fe(OH)_2(PO_4)^{3-}$

high temperature forms: $Fe(OH)_2(H_2PO_4)^-$, $Fe(OH)_3(H_2PO_4)^-$, $Fe(OH)_3(HPO_4)^{2-}$, and $Fe(OH)_4(HPO_4)^{3-}$

Table V presents all of the fitted thermodynamic quantities required to calculate magnetite solubility behavior in alkaline sodium phosphate solutions. This fit produced an overall standard deviation between measured and fitted solubilities of $\pm$ 19%.

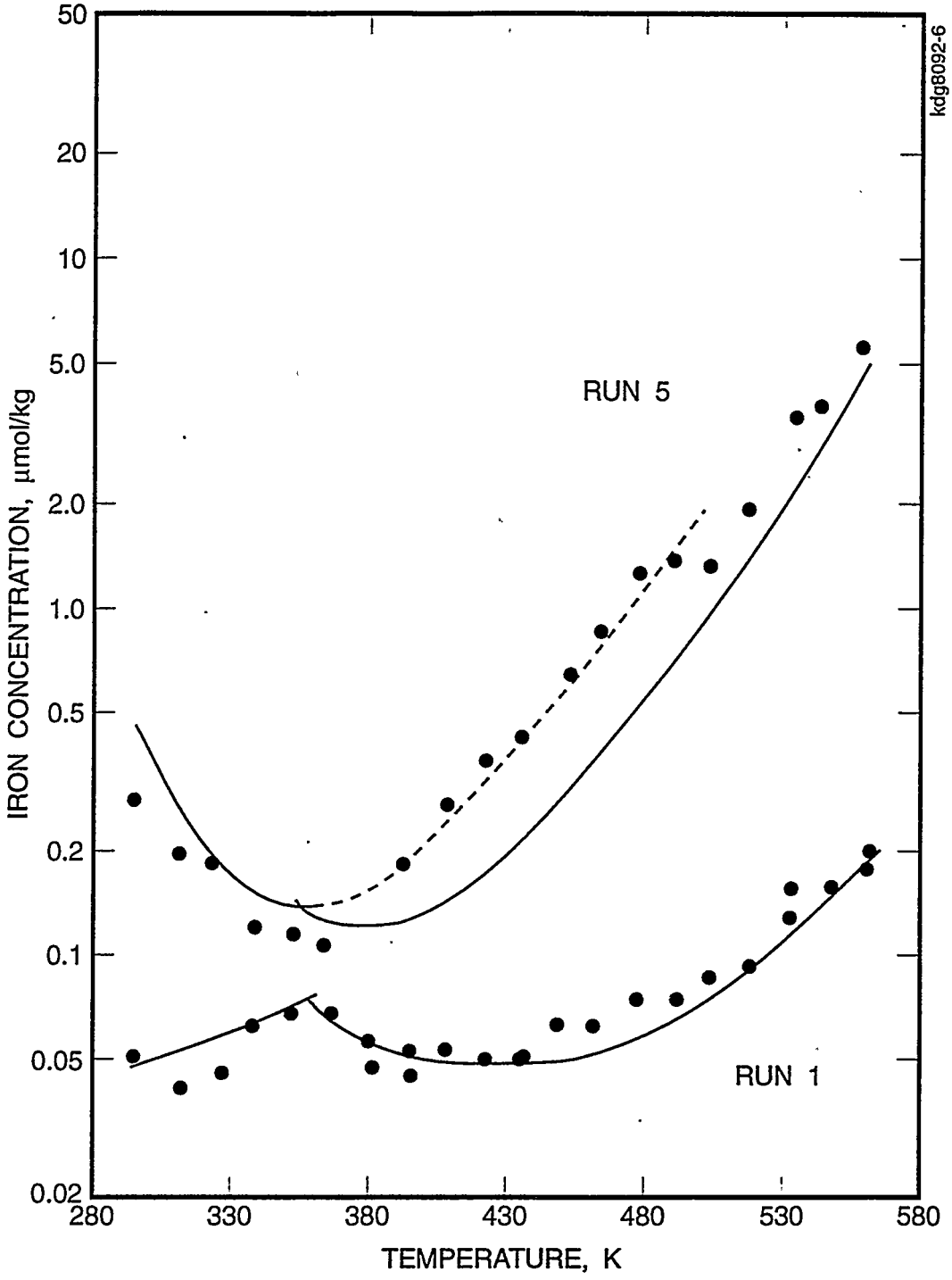

FIGURE 6 Comparison of measured and fitted solubilities of magnetite in sodium phosphate solutions (Na/P = 2.3). Note the delayed $Fe(OH)_2$ solid phase transformation to Fe_3O_4 in Run 5 ($T_o \approx 233°C$).

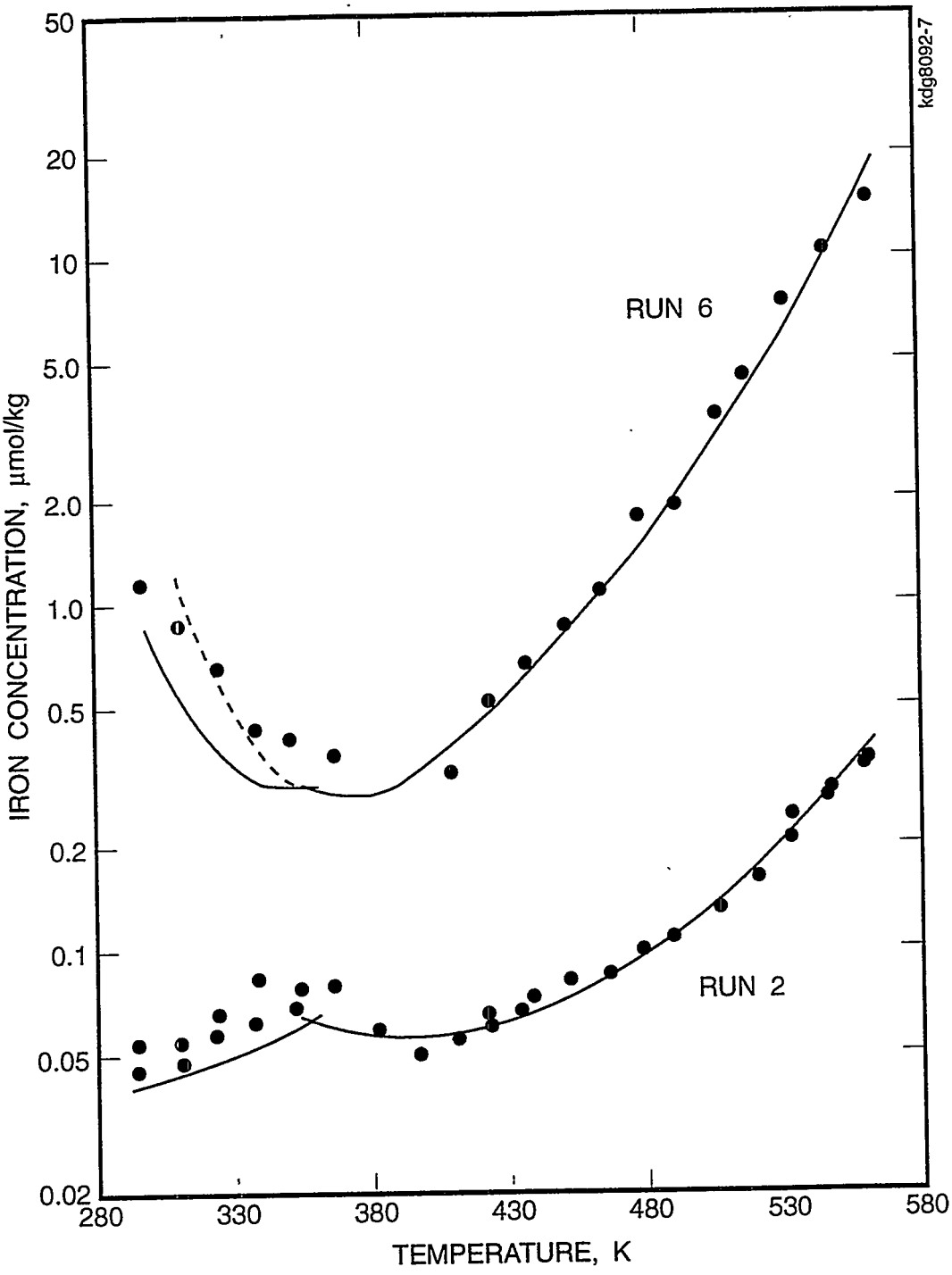

FIGURE 7 Comparison of measured and fitted solubilities of magnetite in sodium phosphate solutions (Na/P = 2.3). Note the apparent phase stability of Fe_3O_4 at low temperatures in Run 6.

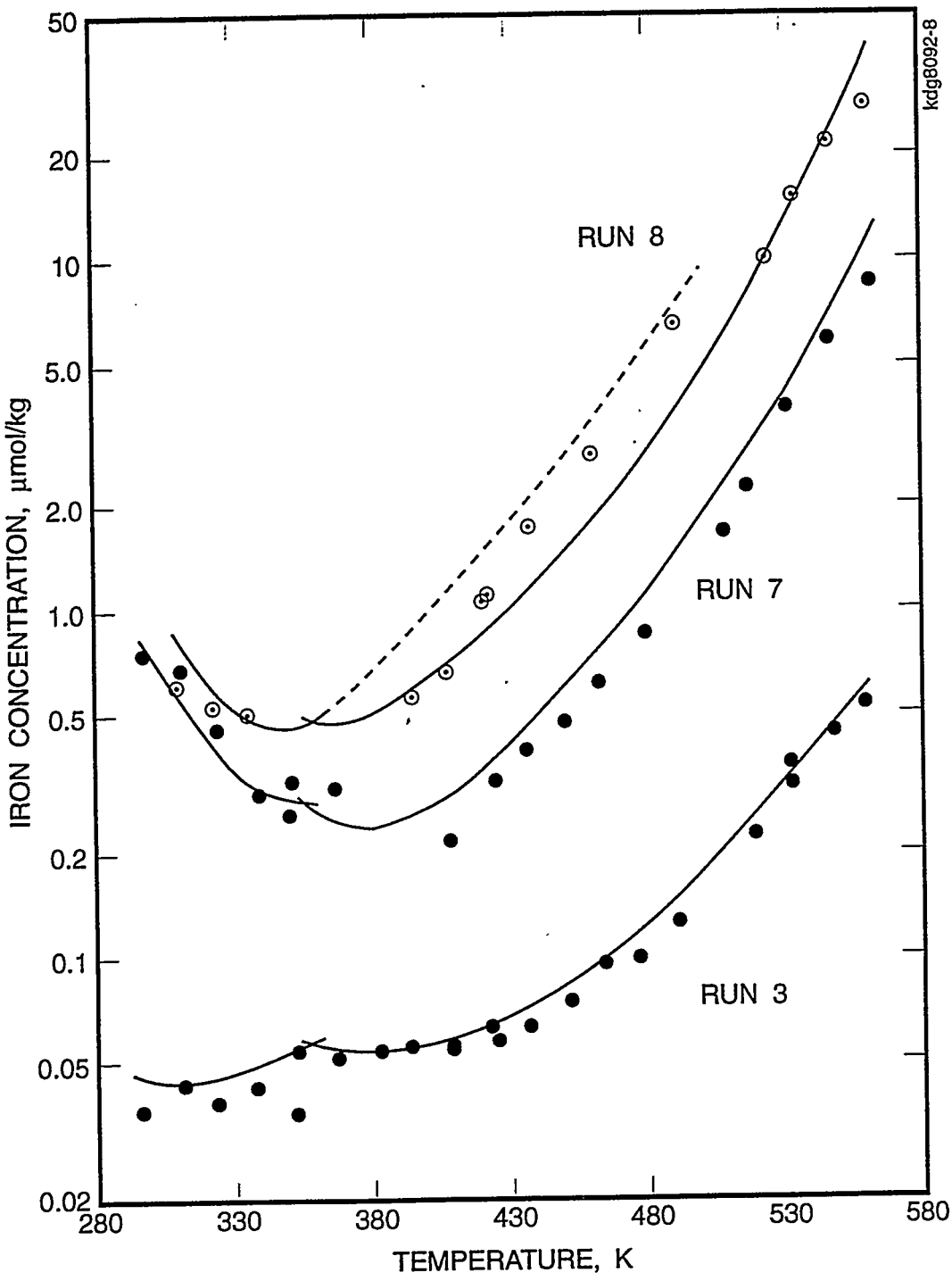

FIGURE 8 Comparison of measured and fitted solubilities of magnetite in sodium phosphate solutions (Na/P = 2.3, Run 3; Na/P = 2.1, Run 7; Na/P = 2.8, Run 8).

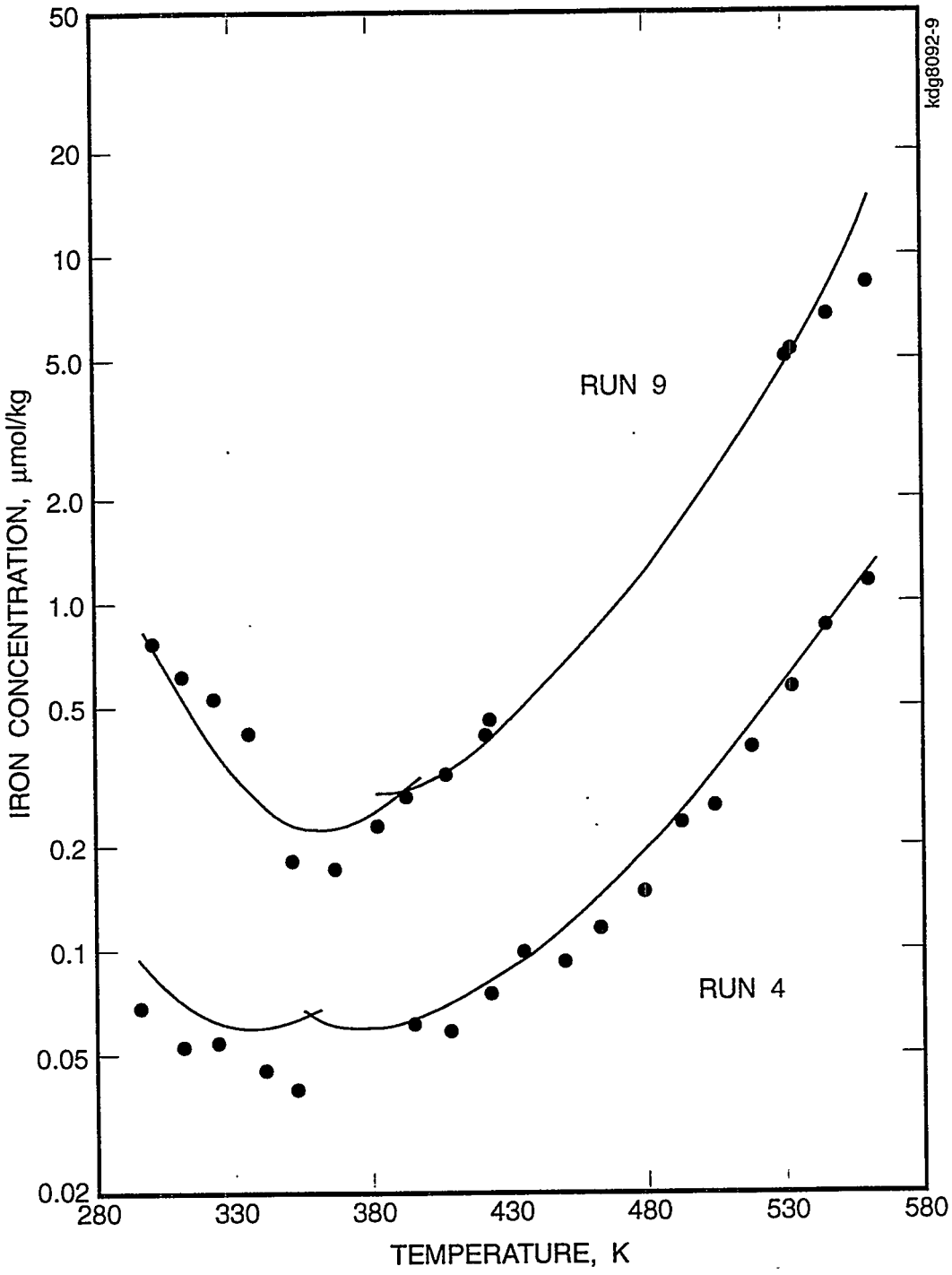

FIGURE 9 Comparison of measured and fitted solubilities of magnetite in sodium phosphate solutions (Na/P = 2.3). The $Fe(OH)_2/Fe_3O_4$ solid phase transformation occurs at 116°C when a higher dissolved hydrogen level is used (779 μm, Run 9).

TABLE V

Thermodynamic Parameters for the Calculation of Magnetite Solubilities in Alkaline Sodium Phosphate Solutions*

Reaction	ΔH°, kJ/mol	ΔS°, J/mol-K	ΔG°(298), kJ/mol
	Hydrolysis		
$Fe(OH)_2(aq) + H_2O \rightleftarrows Fe(OH)_3^- + H^+$	42.90 ±5.30	(-90.85)	69.98
$Fe(OH)_3(aq) + H_2O \rightleftarrows Fe(OH)_4^- + H^+$	19.25 ±0.68	(-119.12)	54.77
	Oxidation		
$Fe(OH)_2(H_2PO_4)^- + H_2O \rightleftarrows Fe(OH)_3(H_2PO_4)^- + ½H_2(g)$	35.59 ±13.15	(62.72)	16.89
	Fe(II) Phosphatocomplexing		
$Fe^{2+} + HPO_4^{2-} \rightleftarrows Fe(HPO_4)(aq)$	-	-	-20.54 ±1.72[9]
$Fe(OH)_2(aq) + H_2PO_4^- \rightleftarrows Fe(OH)(HPO_4)^- + H_2O$	-65.24 ±2.83	-58.46 ±9.10	-47.81 ± 0.26
$Fe(OH)^+ + HPO_4^{2-} \rightleftarrows Fe(OH)(HPO_4)^-$	(9.05)**	(110.29)**	(-23.84)**
$Fe(OH)_2(aq) + HPO_4^{2-} \rightleftarrows Fe(OH)_2(HPO_4)^{2-}$	-42.94 ±12.70	-68.78 ±40.37	-22.43 ±0.97
$Fe^{2+} + H_2PO_4^- \rightleftarrows Fe(H_2PO_4)^+$	-	-	-15.40 ±1.14[9]
$Fe(OH)_2(aq) + H_2PO_4^- \rightleftarrows Fe(OH)_2(H_2PO_4)^-$	-27.66 ±27.70	26.22 ±68.12	-35.48 ±7.42
$Fe(OH)_2(aq) + PO_4^{3-} \rightleftarrows Fe(OH)_2(PO_4)^{3-}$	-50.34 ±14.54	-80.44 ±48.56	-26.36 ±0.67
	Fe(III) Phosphatocomplexing		
$Fe^{3+} + HPO_4^{2-} \rightleftarrows Fe(HPO_4)^+$	-	-	-62.13[32], -46.99[10]
$Fe(OH)_3(aq) + HPO_4^{2-} \rightleftarrows Fe(OH)_3(HPO_4)^{2-}$	-23.37 ±3.86	33.44 ±8.07	-33.34 ±1.48
$Fe(OH)_4^- + HPO_4^{2-} \rightleftarrows Fe(OH)_4(HPO_4)^{3-}$	-42.16 ±2.04	-51.82 ±4.88	-26.71 ±0.67
$Fe^{3+} + H_2PO_4^- \rightleftarrows Fe(H_2PO_4)^{2+}$	-	-	-15.40[32], -19.92[10], -31.00[33]

*Includes refit of higher order hydrolysis reactions from Table IV; remaining equilibria were fixed at their Table IV values. ** $\Delta G(T) = -56546 + 1363.15T - 219.99T\ell nT$ calculated from preceding reaction equilibrium by subtracting ΔG for $H_2PO_4^-$ dissociation and adding ΔG for $Fe(OH)^+$ hydrolysis, i.e., Eq. (22).

DISCUSSION

Dissolution of Magnetite into Fe^{2+}

Initial attempts at fitting the Eq. (1) magnetite dissolution reaction equilibrium for n = 0 to a three parameter thermodynamic model, which allowed for curvature in a single ΔG vs. T correlation, proved unsatisfactory. That is, excessive curvature in the $\Delta G(T)$ correlation was indicated and the fitted $\Delta G°(298)$ value was too low in comparison to expected results, cf, Sweeton and Baes[1] or Tremaine and LeBlanc[2]. This inconsistency was removed by allowing a hydrous Fe(II) oxide phase to exist on the magnetite surface at temperatures below 83°C. Such behavior implied that Fe(II) solubilities at low temperatures were insensitive to changes in dissolved hydrogen levels, i.e., compare Eq. (1) with Eq. (4). An inter-run comparison of iron solubilities between Runs 6 and 9, over the temperature interval 20 - 80°C (see Table II), confirmed approximately no difference despite a factor of three increase in dissolved hydrogen level. Thus, our measurements remain consistent with the result that magnetite solubility behavior at low temperatures is controlled by a surface layer of hydrous Fe(II) oxide.

On the basis of the current analysis, it is seen that the low temperature dissolution reaction equilibrium has a standard free energy change of -62.25 $\pm$1.90 kJ/mol. Literature $\Delta G°$ estimates for the n = 0 form of Eq. (4) are highly dependent on the crystalline state of the $Fe(OH)_2$ solid phase. For example, freshly precipitated, amorphous $Fe(OH)_2$ gives -77.68 $\pm$0.28 kJ/mol[24], while metastable $Fe(OH)_2$ in a relatively active form gives -73.34 $\pm$1.13 kJ/mol[19]. A calculated $\Delta G°$ value for Eq. (4) based on the NBS compilation[22] of standard free energies of formation for Fe^{2+}(aq) and (presumably) fully-crystalline $Fe(OH)_2$

gives -66.66 kJ/mol. Therefore, our result is not inconsistent with the reported literature, considering measurement errors and crystallinity effects.

On the other hand, our extrapolated standard free energy change for magnetite dissolution (Eq. (1)), was found to be $\Delta G°(298) = -65.90 \pm 1.54$ kJ/mol. This value is approximately mid-way between the -68.66 and -62.70 $\pm$0.43 kJ/mol values reported previously by Sweeton and Baes[1] and Tremaine and LeBlanc[2], respectively. Using recent literature values of -1015.23 kJ/mol[25] for the standard free energy of formation for magnetite and -91.21 kJ/mol[21] for the standard free energy of formation for $Fe^{2+}(aq)$ gives $\Delta G°(298) = -68.97$ kJ/mol for Eq. (1). These values agree to within the expected measurement errors.

Free energy changes for the two iron oxide dissolution reactions, Eqs. (1, 4), are plotted in Fig. 10 as functions of temperature. Consistent with the expected behavior of a hydrous oxide phase, a smaller entropy decrease (-49.3 $\pm$24.7 J/mol-K) is observed for Eq. (4). This result contrasts with a larger entropy decrease observed for Eq. (1) at 298 K (-104.3 J/mol-K). The fitted ΔS for Eq. (4), however, is virtually identical to the -47.9 $\pm$6.6 J/mol-K value found by Johnson and Bauman[24] for dissolution of freshly precipitated, amorphous $Fe(OH)_2$.

As shown in Fig. 10, our three parameter expression used to describe the Eq. (1) reaction equilibrium agrees to within 1.2 kJ/mol with the results of Tremaine and LeBlanc over the temperature interval 380 - 560 K. Agreement with the results of Sweeton and Baes is adequate, although deviations as high as 6 kJ/mol are encountered at the higher temperatures. It is noted that our fit of the Eq. (1) equilibrium for n = 0 contained no

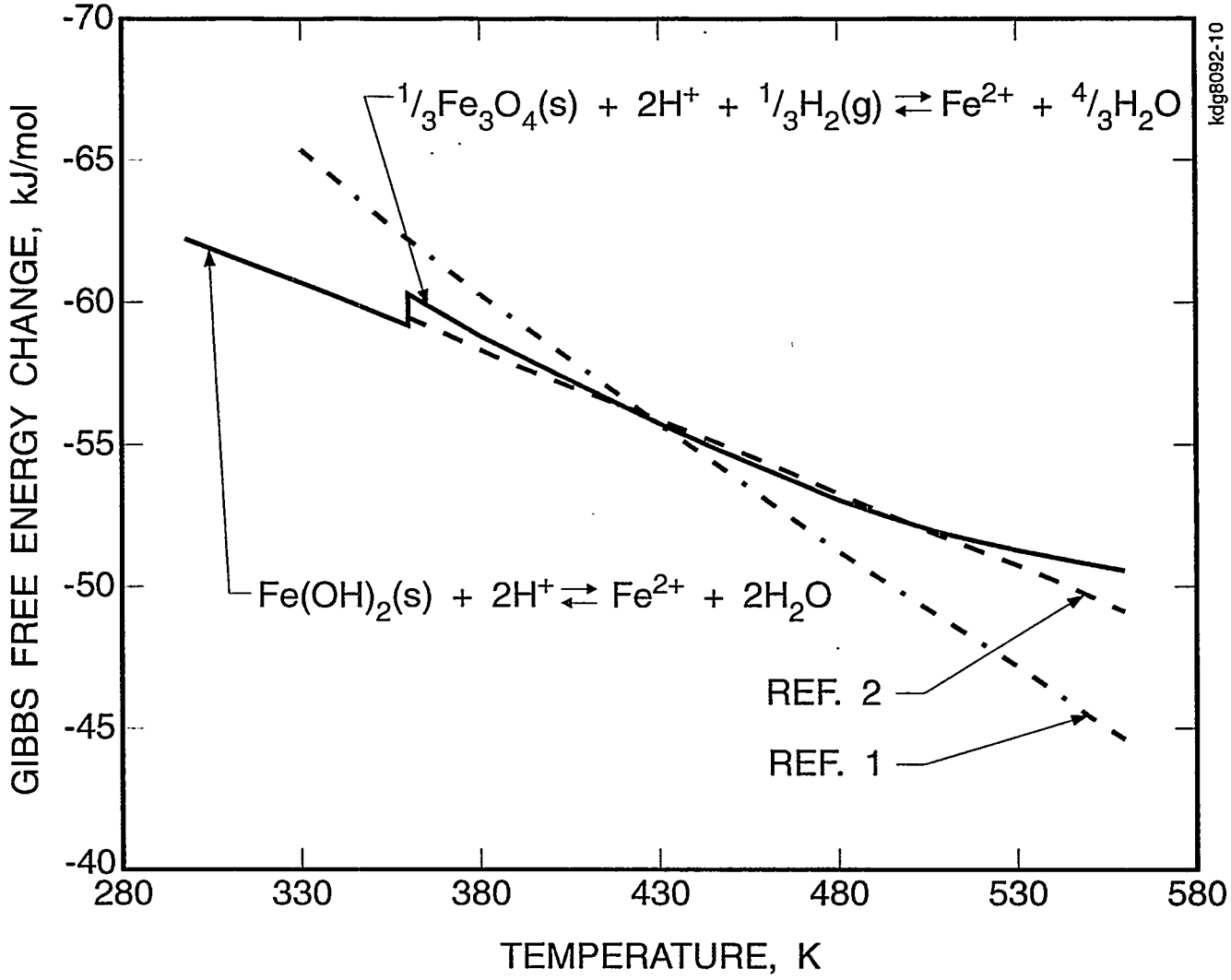

FIGURE 10 Free energy changes measured during magnetite/ferrous hydroxide dissolution to Fe^{2+}. A $Fe(OH)_2/Fe_3O_4$ solid phase transformation occurs at 356 K when $[H_2]$ = 237 μm.

solubility data in the acid pH region and utilized no fitting constraints. Our fitted standard entropy change for Eq. (1) agrees quite well with the -105.8 J/mol-K constraint imposed by Sweeton and Baes[1]. Likewise, the average of our fitted entropy changes for Eq. (1) over the temperature interval 380 - 560 K, -47.0 ±25.4 J/mol-K, also agrees with the -51.6 ±3.3 J/mol-K (constant) value fitted by Tremaine and LeBlanc[2].

Heat capacity effects were also included in the Eq. (1) dissolution reaction equilibrium. Even though small changes in heat capacity were associated with magnetite dissolution, the existence of a large temperature range made it prudent to account for such an effect. A value of 131.3 ±39.4 J/mol-K was fitted for ΔC_p° for Eq. (1). Based on tabulated standard molal heat capacities, ΔC_p°, for magnetite, water, and hydrogen (150.73, 75.29, and 28.82, respectively)[25], it is found that $C_p^\circ(Fe^{2+}(aq)) = 90.8$ J/mol-K. This value is in excellent agreement with an 83 ±10 J/mol-K estimate provided by Tremaine and LeBlanc[2]. Note that when the absolute scale is used (i.e., $C_p^\circ(H^+(aq)) = -71$ J/mol-K [26], $C_p^\circ(Fe^{2+}(aq)) = -51.2$ J/mol-K.

$Fe(OH)_2/Fe_3O_4$ Transformation Temperature

Combination of the two iron oxide dissolution reactions, Eqs. (1, 4), shows that

$$Fe(OH)_2(s) \rightleftarrows 1/3\ Fe_3O_4(s) + 1/3\ H_2(g) + 2/3\ H_2O \qquad (18)$$

Since the equilibrium constant for the above transformation reaction is given by

$$K_{eq} = \{P(H_2)\}^{1/3} \qquad (19)$$

the $Fe(OH)_2/Fe_3O_4$ transformation temperature is described by the temperature (T_o) at which

$$\Delta G_4(T_o) = \Delta G_1(T_o) - (2.3026RT_o/3) \log P(H_2) \qquad (20)$$

Based on the fitted parameters reported in Table IV and a dissolved hydrogen gas pressure of

0.3 atm at 25°C, this thermodynamic threshold is 83°C.

As shown in Eqs. (19, 20), the transformation temperature is affected by the level of dissolved hydrogen. For example, if $P(H_2) = 1$ atm at 25°C (as used by Sweeton and Baes and Tremaine and LeBlanc), the predicted $Fe(OH)_2/Fe_3O_4$ transformation temperature increases to 116°C. Such a high value indicates that the magnetite solubility data reported by these investigators at temperatures below 116°C may not represent true equilibrium solubility data.

Fe(II) Ion Hydrolysis

The distribution of all soluble iron ion aquohydroxocomplexes in solution at saturation is shown in Fig. 11 for magnetite dissolution by a fully-dissociated, univalent, non-complexing alkaline pH reagent (i.e., NaOH). Note the insignificant contribution of Fe(III) ion species at ambient temperature. The standard free energy changes for the first three stepwise hydrolysis reactions of the ferrous ion, as provided by the Table IV analyses, are 51.08 ±2.96, 65.19 and 69.83 kJ/mol, respectively. All three values are in excellent agreement with previously published work[1, 2, 19].

The most reliable room temperature results for the first stepwise hydrolysis reaction

$$Fe^{2+} + H_2O \rightleftarrows Fe(OH)^+ + H^+ \qquad (21)$$

place $\Delta G°(298)$ for Eq. (21) between 52.68 ±0.57[24] and 54.17 ±0.46[27] kJ/mol, and indicate that $Fe(OH)^+$ formation occurs around pH(25°C) = 9.2 - 9.5. Because our solubility database included a feedwater pH condition which maximized $Fe(OH)^+$ concentrations (i.e., 9.3), it was possible to obtain reasonably accurate ΔG estimates for Eq. (21) despite the minor role played by the $Fe(OH)^+$ species. It is noted that Tremaine and

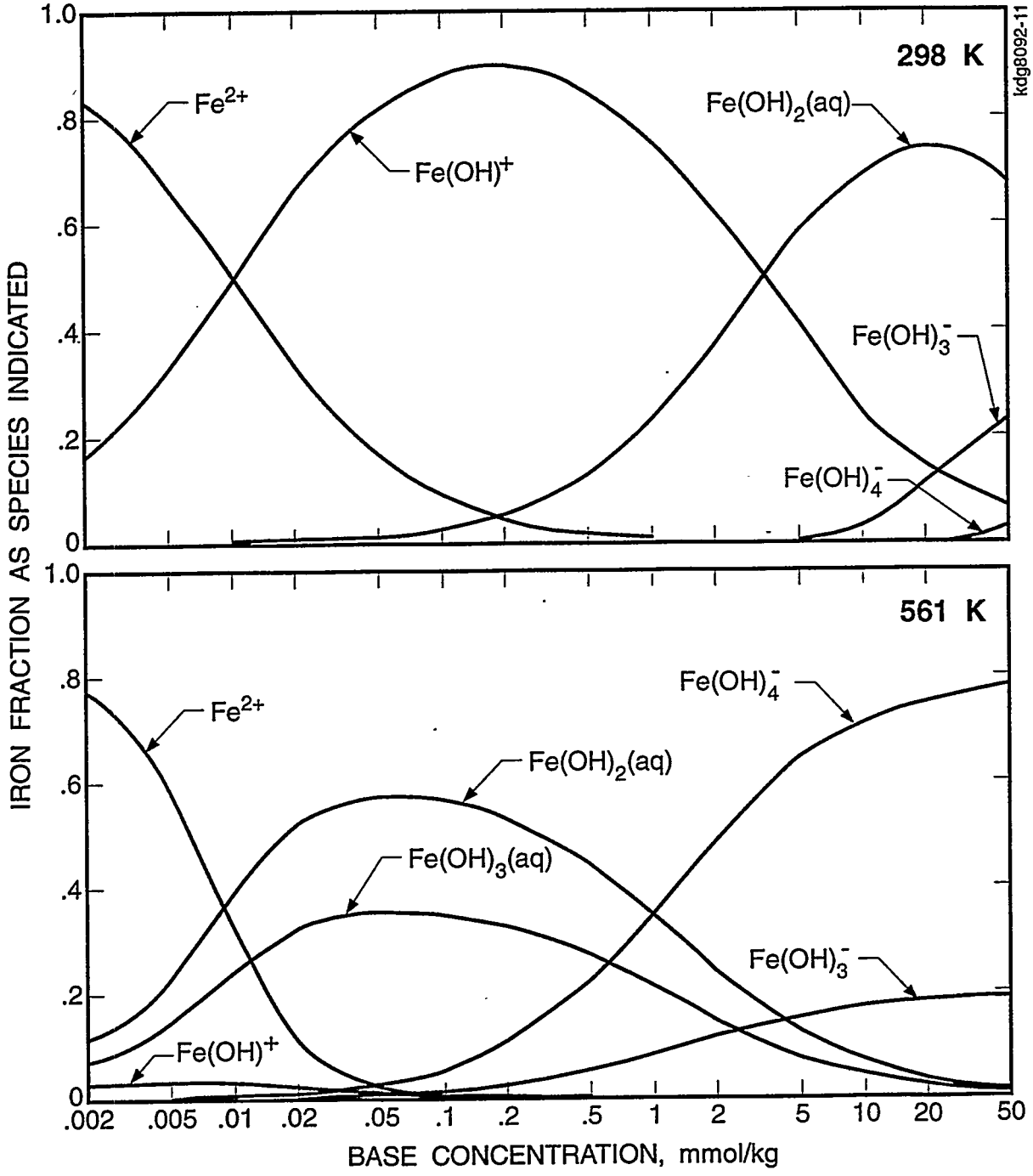

FIGURE 11 Distribution of Fe(II) and Fe(III) ion hydroxocomplexes present in solution at 25°C (top) and 288°C (bottom) for magnetite dissolution in a fully dissociated, univalent, non-complexing pH reagent ($[H_2]$ = 237 μm).

LeBlanc constrained ΔS for Eq. (21) to the value reported by Johnson and Bauman[24]. This constraint resulted in a relatively imprecisely fitted ΔG°(298) for Eq. (21) as 58.1 ± 5.5 kJ/mol[2], and placed $Fe(OH)^+$ formation at pH (25°C) = 10.2.

Relative to the second stepwise hydrolysis reaction

$$Fe(OH)^+ + H_2O \rightleftarrows Fe(OH)_2\,(aq) + H^+ \qquad (22)$$

our ΔG° value agrees quite well with those derived from the two previous magnetite solubility studies, 64.14[1] and 60.33 ±2.55[2] kJ/mol. As mentioned previously, an indirect constraint was placed on the standard free energy change for the third stepwise hydrolysis reaction, Eq. (13), to allow the $Fe(OH)_4^-$ hydroxocomplex to fit the iron solubility increases that occurred around pH = 9.6.

Figure 12 plots the high temperature equilibria for all three Fe(II) ion hydrolysis reactions and compares them with the previous results of Sweeton and Baes[1] and Tremaine and LeBlanc[2]. Although general agreement exists between our results and the previous results, three specific areas of disagreement are noted. First, our fitted equilibrium for Eq. (21) indicates a much greater temperature dependency than reported by Sweeton and Baes[1]. A larger ΔS value is consistent with the results of Tremaine and LeBlanc, although their constrained ΔS value for Eq. (21) is apparently too low and caused their extrapolated ΔG° value to be too high. Our unconstrained ΔG(T) fit for Eq. (21) provides values to within 2 kJ/mol of Johnson and Bauman's[24] and to within 3 kJ/mol of Tremaine and LeBlanc's[2], over their common range of temperature.

Due to the differing ΔG values for the first stepwise hydrolysis reaction, formation of the second hydroxocomplex was illustrated by summing Eqs. (21, 22):

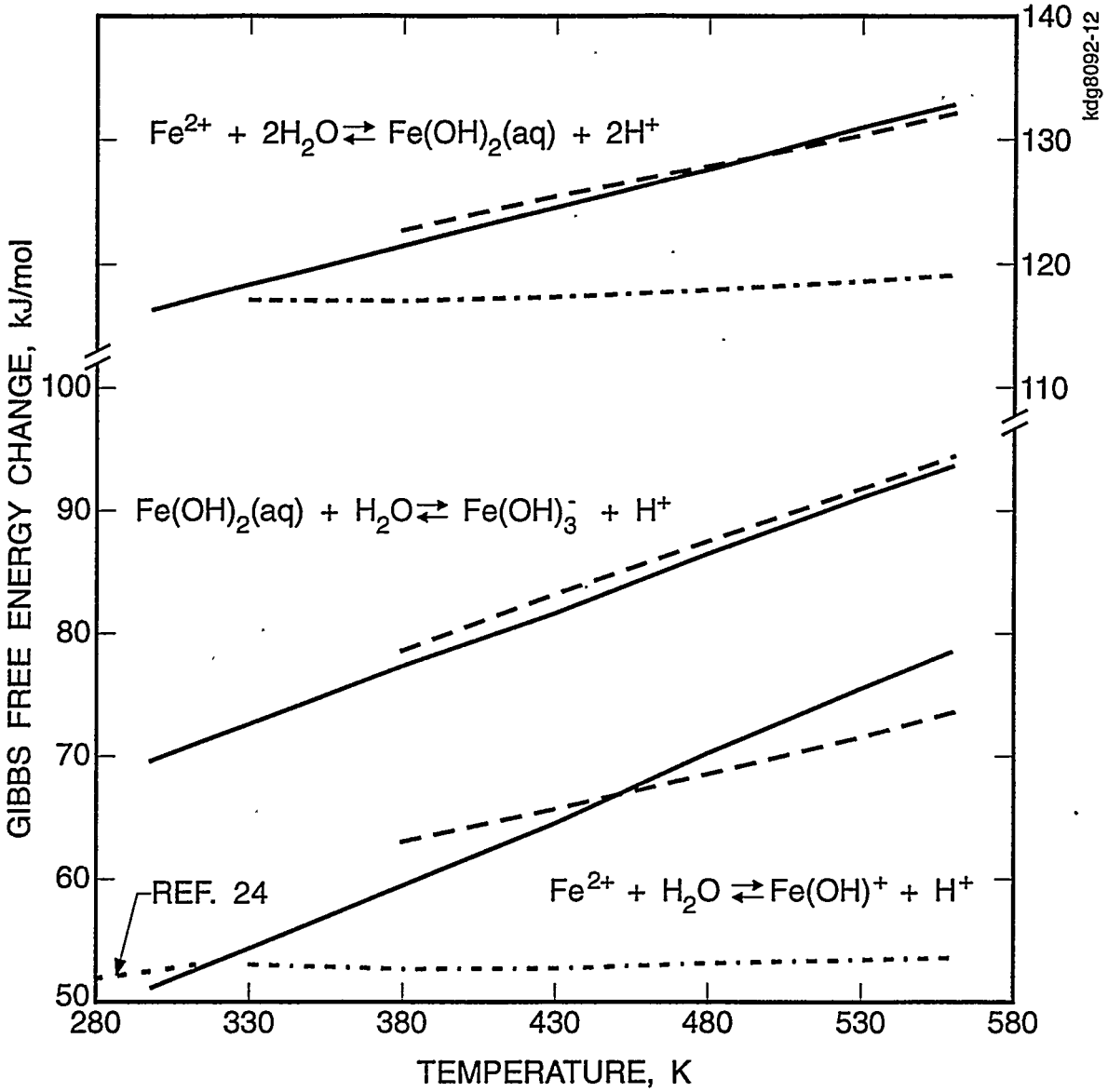

FIGURE 12 Free energy changes determined for Fe(II) ion stepwise hydrolysis reactions. Previous measurements shown by — · — · — (Ref. 1) and — — — (Ref. 2).

$$Fe^{2+} + 2H_2O \rightleftarrows Fe(OH)_2(aq) + 2H^+ \quad (23)$$

Figure 12 shows excellent agreement between our results and those of Tremaine and LeBlanc ($\pm$1 kJ/mol), while Sweeton and Baes' results appear to be an artifact of higher magnetite solubilities (in the alkaline pH region) relative to our measurements and those of Tremaine and LeBlanc, and are indicative of a probable source of low level contamination. Thirdly, our free energy changes for Eq. (13) support the results of Tremaine and LeBlanc, while the results of Sweeton and Baes are rejected as being inappropriate for the intended hydrolysis reaction. The virtual coincidence of our results with those of Tremaine and LeBlanc is caused primarily by a fit of the same source of $Fe(OH)_3^-$ solubility data, rather than inclusion of an additional source of solubility measurements.

Consistent with the above discussion, we conclude that the ΔG vs. T behavior reported by Sweeton and Baes for the first three stepwise hydrolysis reactions of the Fe(II) ion, as well as Tremaine and LeBlanc's ΔG° result for the first stepwise hydrolysis reaction, are inaccurate.

Amminocomplexing

The importance of iron ion aquohydroxoamminocomplexes is illustrated in Fig. 4 where the fitted solubilities of magnetite are compared against predictions made using Tremaine and LeBlanc's fitted parameters and amminocomplexing is neglected; see dashed lines. As noted previously, mutually consistent sets of ammino- (and hydroxo-) complexing equilibria were derived by combining the present magnetite solubility measurements in ammonium hydroxide (Runs 10, 11/11A) with those of Tremaine and LeBlanc's in sodium hydroxide; see Table IV. The validity of this analytical approach rests on the assumption

that the two databases are unbiased relative to each other. Although we did not determine Fe_3O_4 solubilities in sodium hydroxide, Run 10, conducted with ammonia levels not expected to yield significant iron ion amminocomplexing, serves as a validity check.

As shown in Figs. 4 and 5, consistency between the two databases was achieved by recognizing the presence of a single ammine complex: $Fe(OH)(NH_3)^+$. Conversely, if amminocomplexing did not occur during Run 10, then an alternate explanation would be that our solubility measurements were biased high by ~ 10% relative to those of Tremaine and LeBlanc's. Since our run-to-run reproducibility was approximately ±20%, we conclude that a bias correction is not warranted.

Our fitted amminocomplexing equilibrium is dependent on the magnetite solubility levels reported by Tremaine and LeBlanc in the pH region of minimum solubility. We believe that this "baseline" condition is warranted because: (1) the Run 10 results are consistent with solubility predictions based on Tremaine and LeBlanc's fitted parameters (where ammine complexes contribute < 10%), and (2) the higher minimum iron concentrations observed in other magnetite solubility studies conducted in non-complexing bases[1, 28, 29] appear to be caused by experimental artifacts such as time-dependent phenomena (discussed by Tremaine and LeBlanc) or low level interference (previously discussed). The magnetite solubility measurements of Lambert et al.[30], after accounting for decay and higher hydrogen levels, are also consistent with the present analysis. A subsequent magnetite solubility study performed by Lambert et al.[31] at room temperature found iron concentrations to be independent of dissolved hydrogen level (an expected result of the present analysis).

The most probable reason, therefore, that our magnetite solubilities in Runs 11/11A (0.027 μm at 250°C) are higher than predicted based on application of Tremaine and LeBlanc's fitted parameters (0.013 μm) is due to the presence of ammine complexes. Given the ammonia levels of Run 11, significant concentrations of iron ion amminocomplexes will be present at 250°C if free energies of amminocomplexing are on the order of -32 kJ/mol. Note that application of Sweeton and Baes' fitted parameters to the Run 11/11A conditions results in a predicted iron concentration of 0.072 μm at 250°C.

Within the context of an overall hydroxoamminocomplexing reaction sequence

$$Fe(OH)_n^{2-n} + aNH_3 \rightleftarrows Fe(OH)_n(NH_3)_a^{2-n} \qquad (24)$$

the use of sub-mm ammonia concentrations in the present investigations limited consideration to $a \leq 1$. Our fitted $\Delta G^\circ = -18.8 \pm 2.3$ kJ/mol for the $n = 1$ form of Eq. (24) is within 5 kJ/mol of the -13.6 kJ/mol value[11] estimated for the $n = 0$ form of Eq. (24). Therefore, these (room temperature) equilibria are not significantly affected by hydrolysis.

Complex formation is favored at elevated temperatures, since Osman et al.[23] indicate that an entropy increase accompanies the n=0 complexing reaction ($\Delta S = 2.5 \pm 5.1$ J/mol-K). Our fitted ΔS value for the $n = 1$ form of Eq. (24), i.e., $\Delta S = 125.3 \pm 30.7$ J/mol-K, accounts for significant concentrations of the $Fe(OH)(NH_3)^+$ species at elevated temperatures. This value would be reduced considerably if the n=2 equilibrium for Eq. (24) were to be included in the analysis. However, our database is insufficient to provide a meaningful fit for inclusion of the $Fe(OH)_2(NH_3)(aq)$ species. Additional magnetite solubility measurements, employing a broader range of ammonia concentrations, are needed to resolve this issue.

Phosphatocomplexing

The distribution of all iron ion hydroxo- and phosphatocomplexes present in sodium phosphate solutions (nominal 2.3 Na/P ratio with 237 μm hydrogen) is shown in Fig. 13. Because solution pH, hence hydrolytic state of the soluble iron ions was controlled by the sodium phosphate concentration, it was not possible to complex measurable levels of Fe^{2+}, Fe^{3+}, $Fe(OH)^{2+}$, or $Fe(OH)_2^+$ ions in the present experimental program. As indicated in Table V, both Fe(II) and Fe(III) ions participated in the phosphatocomplexing reactions.

The standard free energy changes encountered during incorporation of the HPO_4^{2-} ion ligand into the sequence of Fe(II) ion hydroxocomplexes were found to be -23.84 and -22.43 $\pm$0.97 kJ/mol for the respective $Fe(OH)^+$ and $Fe(OH)_2$(aq) ions. These values compare favorably with ΔG° = -20.54 $\pm$1.72 kJ/mol reported for the complexing of HPO_4^{2-} by the unhydrolyzed Fe^{2+} ion[9], and indicate that standard free energies of phosphatocomplexing are relatively insensitive to changes in hydrolytic state of the Fe(II) ion. On the other hand, ΔG° values found for phosphatocomplexing of the HPO_4^{2-} ion with Fe(III) hydroxocomplexes exhibit a considerable dependency on hydrolytic state: -33.34 $\pm$1.48 kJ/mol for $Fe(OH)_3$(aq) and -26.71 $\pm$0.67 kJ/mol for $Fe(OH)_4^-$. The available literature indicates that HPO_4^{2-} complexing with the unhydrolyzed Fe^{3+} ion is even more stabilizing, as ΔG° estimates range between -47.0[10] and -62.1[32] kJ/mol. Therefore, an increase in ΔG° by approximately 7 kJ/mol per OH^- ligand is indicated.

The above complexing behavior of the Fe(II) and Fe(III) ions is illustrated in Fig. 14. As a means to facilitate comparisons between phosphato- and hydroxo-complexing, the iron ion hydrolysis reactions were recast in a form that introduces the hydroxyl ion as the

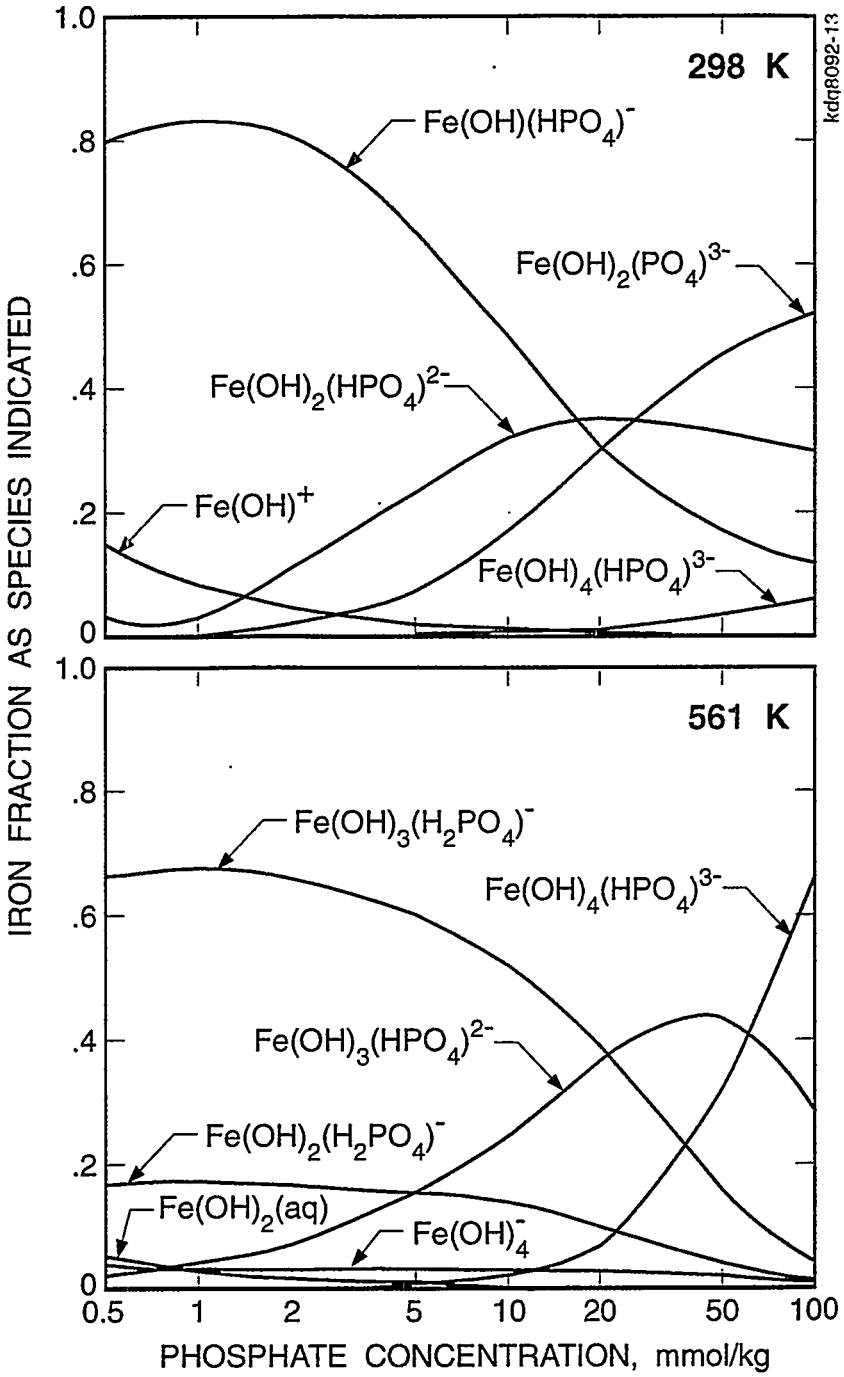

FIGURE 13 Distribution of Fe(II) and Fe(III) ion complexes present in solution at 25°C (top) and 288°C (bottom) for magnetite dissolution in sodium phosphate solutions (Na/P = 2.3, $[H_2]$ = 237 μm).

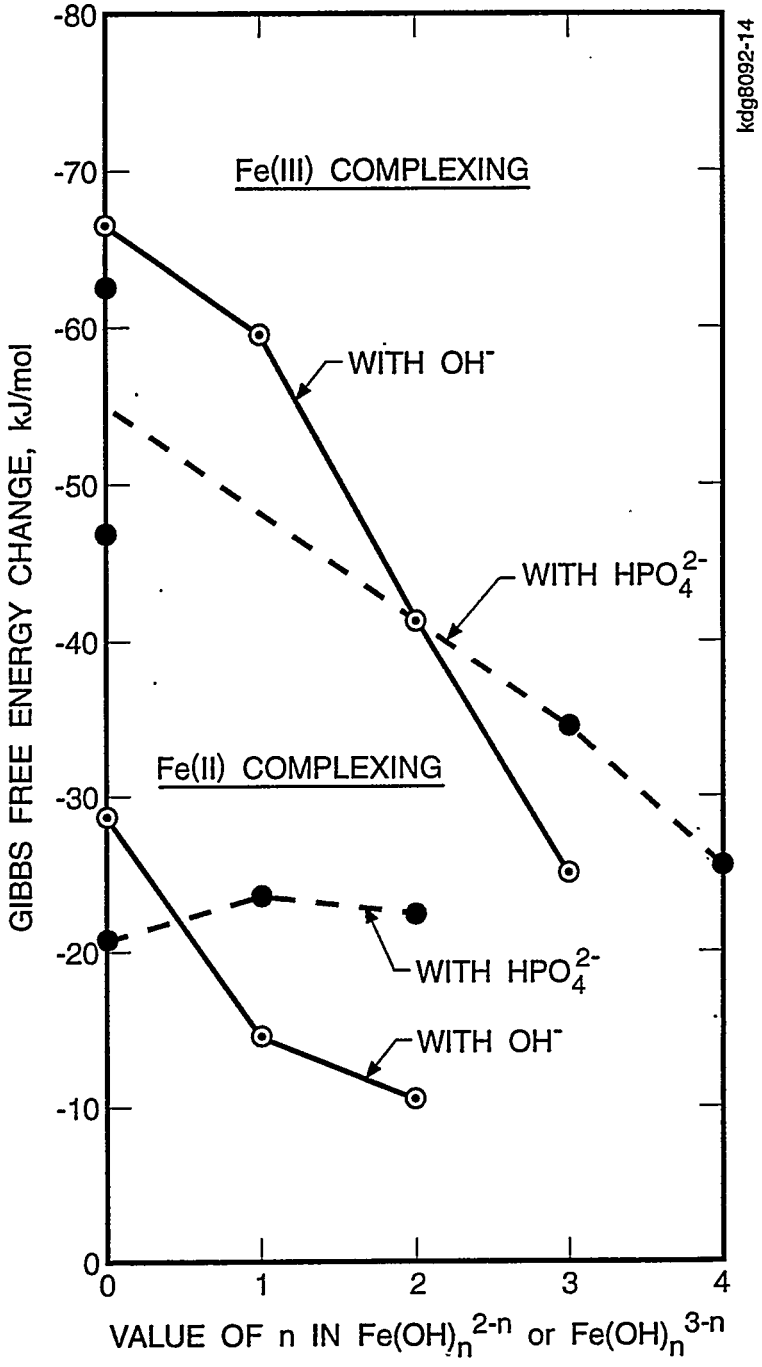

Figure 14 Effect of iron ion hydrolytic state on standard free energies of complexing with OH^- and HPO_4^{2-} ion ligands.

complexing ligand:

$$Fe(OH)_n^{(2-n)+} + OH^- \rightleftharpoons Fe(OH)_{n+1}^{(1-n)+} \quad (25)$$

$$Fe(OH)_m^{(3-m)+} + OH^- \rightleftharpoons Fe(OH)_{m+1}^{(2-m)+} \quad (26)$$

Standard free energy changes for the lower order Fe(III) ion hydrolysis reactions were taken from Baes and Mesmer[19]. Consistent with the greater charge on the HPO_4^{2-} ion relative to the OH^- ion, iron ion phosphatocomplexes are more stable than those of their hydroxo-complexes (i.e., $\Delta G°$s are more negative).

The low temperature portions of Runs 6 - 8, which had the same total phosphate concentrations but varied the relative contribution of HPO_4^{2-} and PO_4^{3-}, provided (limited) evidence for the presence of a higher order anionic phosphatocomplex of the Fe(II) ion. Extrapolation of our previously-fitted hydrolytic and phosphatocomplexing sequences suggests the possibility of $Fe(OH)_3(HPO_4)^{3-}$ and/or $Fe(OH)_2(PO_4)^{3-}$ formation.

$$Fe(OH)_3^- + HPO_4^{2-} \rightleftharpoons Fe(OH)_3(H_2PO_4)^{3-} \quad (27)$$

$$or\ Fe(OH)_2(aq) + PO_4^{3-} \rightleftharpoons Fe(OH)_2(PO_4)^{3-} \quad (28)$$

Since it was not possible to simultaneously fit both species in the same temperature region (as discussed previously), separate fits were performed using Eq. (27) or (28). Both fits provided the same overall precision. However, only the Eq. (28) equilibrium was included in Table IV. This action was taken because the lowest temperature region of Runs 6 - 8 contained the concentration in equalities: $[Fe(OH)_2(aq)] > [Fe(OH)_3^-]$ and $[PO_4^{3-}] > [HPO_4^{2-}]$. Therefore, the indicated magnitude of the thermodynamic parameters for Eq. (28) were smaller than for Eq. (27). A more complex fit, which accounts for a transformation

between the two, was not pursued.

Entropy decreases associated with the Fe(II)-HPO_4 phosphatocomplexing reactions caused these species to become less important at elevated temperatures, while entropy increases associated with the Fe(III)-HPO_4 phosphatocomplexing reactions caused these species to increase in importance at elevated temperatures (relative to their precursor hydroxocomplexes). The significance of this result is that Fe(III)-HPO_4 complexes control magnetite solubility behavior rather than the Fe(III)-OH and Fe(II)-OH hydrolytic complexes usually present at elevated temperatures. Therefore, when the solubility limit is exceeded in concentrated alkaline sodium phosphate solutions, a sodium ion salt of a Fe(III) ion mixed phosphatohydroxocomplex can precipitate, rather than magnetite. Additional work at this laboratory has already defined this phase boundary (phosphate concentration, temperature, and Na/P ratio) and established the identity of the precipitated phase, i.e., $Na_4Fe(OH)(PO_4)_2.1/3NaOH$[4]. This result indicates that the preferred Fe(III) ion high-temperature, anionic complex ($Fe(OH)_4(HPO_4)^{3-}$) undergoes a second complexing reaction (probably with the $H_2PO_4^-$ ion) prior to precipitation. Conversely, in concentrated sodium phosphate solutions having lower alkalinities (such as provided by solutions with $Na/P \leq 2$) the predicted dominance of the Fe(II) ion phosphatocomplex, $Fe(OH)_2(H_2PO_4)^-$, would lead to the precipitation of maricite:

$$Na^+ + Fe(OH)_2(H_2PO_4)^- \rightleftarrows NaFePO_4(s) + 2H_2O \qquad (29)$$

Thus, complementary magnetite phase stability investigations provide indirect support for the present Fe(II)/Fe(III) redox and phosphatocomplexing analyses.

Fe(II) Ion Oxidation

Fe(II) ion hydrolytic phenomena were shown to increase the stability of the Fe(III) ion state relative to the Fe(II) ion state. Fig. 15 compares thermodynamic equilibria for the series of redox reactions, written in a 'hydrolytic' form:

$$Fe(OH)_n^{2-n} + H_2O \rightleftarrows Fe(OH)_{n+1}^{2-n} + \tfrac{1}{2}H_2(g) \quad (30)$$

where n = 0 - 3. Free energy changes for the n=0 and 1 forms of Eq. (30) were calculated from compiled data[22]; those for n = 2 and 3 were taken from Table IV. Fig. 15 shows that hydrolysis, caused by increases in solution pH, shifts the redox equilibria by an average of 24 kJ/mol for each stepwise increase in hydrolysis. This shift is sufficient to cause the Fe(III) ion state to become the stable state of dissolved iron in alkaline solutions in spite of the presence of dissolved hydrogen.

Phosphatocomplexing also alters stabilities of the Fe(II) ion state relative to the Fe(III) ion state. Fig. 16 compares free energy changes for the series of Fe(II)/Fe(III) redox equilibria involving hydroxophosphatocomplexes that contain a hydrogenphosphate ion ligand (HPO_4^{2-}):

$$Fe(OH)_n(HPO_4)^{n-} + H_2O \rightleftarrows Fe(OH)_{n+1}(HPO_4)^{n-} + \tfrac{1}{2}H_2(g) \quad (31)$$

where n= 0 - 2. Standard free energy changes for the n = 0 and 1 forms of Eq. (31) were calculated by combining the Table V equilibria for Fe(II) complexing with estimated ΔG° values for Fe(III) complexing via:

$$Fe(OH)^{2+} + HPO_4^{2-} \rightleftarrows Fe(OH)(HPO_4)(aq) \quad (32)$$

and

$$Fe(OH)_2^{+} + HPO_4^{2-} \rightleftarrows Fe(OH)_2(HPO_4)^{-} \quad (33)$$

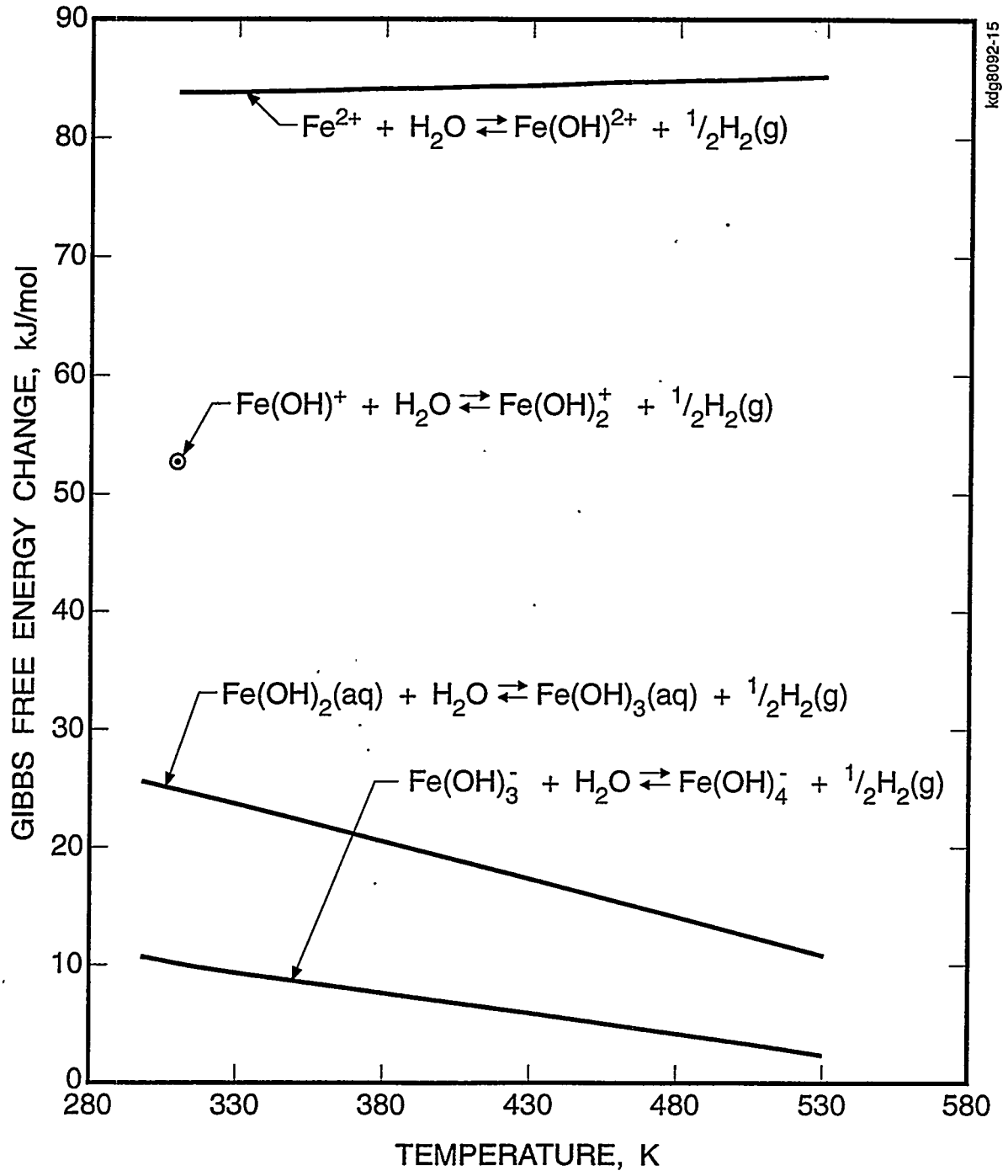

FIGURE 15 Effect of hydrolysis on ferrous ion oxidation reaction equilibria.

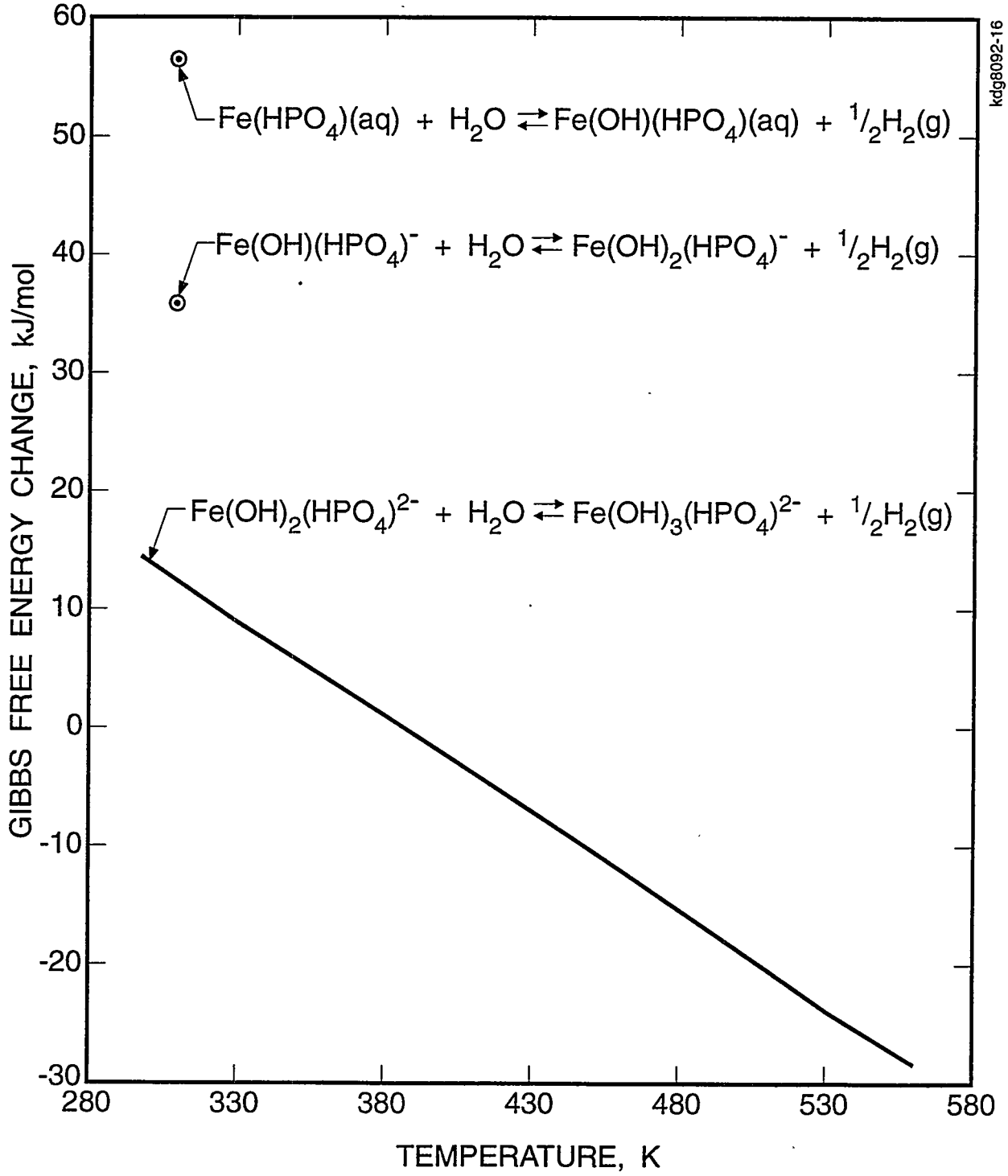

FIGURE 16 Effect of phosphatocomplexing on ferrous ion oxidation reaction equilibria

based on the observed ΔG° dependency upon Fe(III) ion hydrolytic state shown in Fig. 14 (i.e., -48.0 and -41.5 kJ/mol for Eqs. (32, 33), respectively). Free energy changes for the n=2 form of Eq. (31) were taken from a combination of Table V equilibria. These results demonstrate that the addition of an HPO_4^{2-} ligand to a Fe(II) ion hydroxocomplex containing two (or more) OH^- ion ligands extends the temperature region in which ferric ion forms are more stable than their ferrous ion counterparts, i.e., compare Figs. 15 and 16.

By way of closure, Table VI provides a summary of thermochemical properties of known species in the system Fe_3O_4-P_2O_5-H_2O. The new values supplied for hydrous Fe(II) and Fe(III) oxides ensure that these phases are stable in aqueous solutions at ambient temperature relative to the anhydrous forms, Fe_3O_4 and Fe_2O_3, respectively.

TABLE VI

Thermochemical Parameters for Species in the Fe_3O_4-P_2O_5-H_2O System

Species	$C_p°(298)$ J-mol^{-1}-K^{-1}	$S°(298)$ J-mol^{-1}-K^{-1}	$\Delta H_f°(298)$ J-mol^{-1}	$\Delta G_f°(298)$ J-mol^{-1}	Ref.
Fe(s)	24.98	27.28	0	0	[25]
$Fe(OH)_2$(s)	-	84.0	-583.39	-500.16	a
Fe_3O_4(s)	150.73	146.15	-1118.38	-1015.23	[25]
Fe_2O_3 (hematite)	103.87	87.40	-824.25	-742.29	[25]
FeO(OH) (goethite)	69.8[b]	75.8	-556.52	-490.34	[34]
H_2(g)	28.84	130.68	0	0	[25]
O_2(g)	29.38	205.15	0	0	[25]
H_2O(aq)	75.29	69.95	-285.83	-237.14	[25]
H^+(aq)	-71	-22.2	0	0	[26, 35]
Fe^{2+}(aq)	-51.2	-149.6	-88.69	-88.14	a
$Fe(OH)^+$(aq)	-	-162.9	-354.83	-274.18	a
$Fe(OH)_2$(aq)	-	-29.2	-563.08	-446.13	a
$Fe(OH)_3^-$(aq)		-28.7	-806.40	-613.42	a
Fe^{3+}(aq)		-346.9	-50.21	-16.74	[21]
$Fe(OH)^{2+}$(aq)		-150.6	-292.55	-241.58	[19]
$Fe(OH)_2^+$(aq)		-	-	-458.82	[19]
$Fe(OH)_3$(aq)		38.1	-804.81	-657.86	a
$Fe(OH)_4^-$(aq)		10.9	-1071.46	-840.22	a
P(s)	23.8	41.09	0	0	[22]
$H_2PO_4^-$(aq)	37	72.4	-1308.8	-1130.8	[36, 14]
HPO_4^{2-}(aq)	-112	-32.6	-1305.5	-1089.7	[36, 15]
PO_4^{3-}(aq)	-283	-153.6	-1277.4	-1018.8	[36, 22]
$Fe(H_2PO_4)^+$(aq)		-	-	-1234.34	[9]
$Fe(OH)_2(H_2PO_4)^-$(aq)		68.0	-1899.54	-1611.90	a
$Fe(HPO_4)$(aq)		-	-	-1198.38	[9]

Species	$C_p°(298)$ J-mol^{-1}-K^{-1}	$S°(298)$ J-mol^{-1}-K^{-1}	$\Delta H_f°(298)$ J-mol^{-1}	$\Delta G_f°(298)$ J-mol^{-1}	Ref.
$Fe(OH)(HPO_4)^-(aq)$		-84.6	-1651.29	-1387.72	a
$Fe(OH)_2(HPO_4)^{2-}(aq)$		-130.0	-1911.52	-1558.26	a
$Fe(OH)_2(PO_4)^{3-}(aq)$		-263.0	-1890.82	-1491.28	a
$Fe(H_2PO_4)^{2+}(aq)$	-	-	-	-1165.2	[10 + 32]
$Fe(OH)_3(H_2PO_4)^-(aq)$		135.2	-2149.78	-1832.14	a
$Fe(HPO_4)^+(aq)$		-	-	-1161.0	[10 + 32]
$Fe(OH)_3(HPO_4)^{2-}(aq)$		40.0	-2133.68	-1780.89	a
$Fe(OH)_4(HPO_4)^{3-}(aq)$		-72.7	-2419.06	-1956.63	a

---

[a]This work. [b]Estimated from Wagman et al.[22] assuming heat capacities for hematite and goethite are in the same proportion as those for corundum and diaspore. Results of Schmalz[34] recalculated to give $\Delta G = 8870 - 259.7T + 39.62T\ell nT$, J/mol (hematite) for hematite hydration reaction.

REFERENCES

1. F.H. Sweeton and C.F. Baes, J. Chem. Thermodyn. 2, 479 (1970)
2. P.R. Tremaine and J.C. LeBlanc, J. Solution Chem. 9, 415 (1980)
3. S.E. Ziemniak, M.E. Jones and K.E.S. Combs, J. Solution Chem. 18, 1133 (1989)
4. S.E. Ziemniak and E.P. Opalka, in Proc. Sixth International Symposium on Environmental Degradation of Materials in Nuclear Power Systems - Water Reactors, eds., R.E. Gold and E.P. Simonen (The Minerals, Metals & Materials Society, Warrendale, PA, 1993), p. 929
5. E.C. Potter and G.M.W. Mann, in Proceedings of the First International Congress on Metallic Corrosion, Butterworths, London (1962), p. 417
6. E.M. Field and D.R. Holmes, Corros. Sci. 5, 361 (1965)
7. Private communication with J. Chera (GE Corporate R&D Center)
8. N.S. McIntyre and D.G. Zetaruk, Anal. Chem. 49, 1521 (1977)
9. J.O. Nriagu, Geochim. Cosmochim. Acta 37, 2357 (1972)
10. H. Galal-Gorchev and W. Stumm, J. Inorg. Nucl. Chem. 25, 567 (1963)
11. K.B. Yatsimirskii, J. Gen. Chem. USSR 24, 1485 (1954)
12. F.H. Sweeton, R.E. Mesmer and C.F. Baes, J. Solution Chem. 3, 191 (1974)
13. B.F. Hitch and R.E. Mesmer, J. Solution Chem. 5, 667 (1976)
14. R.E. Mesmer and C.F. Baes, J. Solution Chem. 3, 307 (1974)
15. N.C. Treloar, Central Electricity Research Laboratory Report RD/L/N 270/73 (1973). (See WAPD-TM-1302, March 1979)

16. L.O. Gilpatrick and H.H. Stone, Oak Ridge National Laboratory Reports ORNL-3127 (1961) and ORNL-3262 (1962)

17. W.L. Marshall and E.V. Jones, J. Phys. Chem. 70, 4028 (1966)

18. D.L. Marquardt, J. Soc. Indust. Appl. Math. 2, 431 (1963)

19. C.F. Baes and R.E. Mesmer, The Hydrolysis of Cations, Wiley-Interscience, New York (1976)

20. K.H. Gayer and A.B. Garrett, J. Amer. Chem. Soc. 72, 3921 (1950)

21. J.W. Larson, P. Cerutti, H.K. Garber, and L.G. Hepler, J. Phys. Chem. 72, 2902 (1968)

22. D.D. Wagman, W.H. Evans, V.B. Parker, R.H. Schumm, I. Halow, S.M. Bailey, K.L. Churney, and R.L. Nuttall, The NBS Tables of Chemical Thermodynamic Properties, J. Phys. Chem. Ref. Data 11, Suppl. No. 2 (1982)

23. M.M. Osman, T.M. Salem and N.J.L. Gayed, Inorg. Chimica Acta 58, 233 (1981)

24. G.K. Johnson and J.E. Bauman, Inorg. Chem. 17, 2774 (1978)

25. I. Barin, Thermochemical Data of Pure Substances, VCH Verlagsgesellschaft, Weinheim (1989)

26. M.H. Abraham and Y. Marcus, J. Chem. Soc., Faraday Trans. 1, 82, 3255 (1986)

27. R.E. Mesmer, Inorg. Chem. 10, 857 (1971)

28. G.A. Kanert, G.W. Gray, and W.G. Baldwin, Report AECL-5528, Atomic Energy of Canada, Ltd., (1976)

29. M.A. Styrikovich, O.I. Martynova, I.F. Kobyakov, V.L. Men'shikova, and M.I. Reznikov, Therm. Eng. 19, 127 (1972)

30. I. Lambert, J. Montel, P. Beslu, and A. Lalet, in Thermodynamics of Nuclear Materials 1979, International Atomic Energy Agency, Vienna (1980), p. 89

31. I. Lambert, J. Montel, and P. Courvoisier, in Proc. Second International Conference on Water Chemistry of Nuclear Reactor Systems, British Nuclear Energy Society, London (1980), p. 31

32. S.C. Lahiri, J. Ind. Chem. Soc. 42, 715 (1965)

33. J.O. Nriagu, Amer. J. Sci. 272, 476 (1972)

34. R.F. Schmalz, J. Geophys. Res. 64, 575 (1959)

35. C.M. Criss and J.W. Cobble, J. Amer. Chem. Soc. 86, 5390 (1964)

36. J.W. Larson, K.G. Zeeb and L.G. Hepler, Can. J. Chem. 60, 2141 (1982)